Supplementary Information (SI) for Journal of Materials Chemistry A.

Supporting Information

Multi-Capture Site Design in a Bifunctional Zr-MOF for Broad-Spectrum and Efficient Removal of Short- and Long-Chain PFAS

Qiang Bi, [a] Shiping Zhao, [a]Yumiao Zhang, [a] Cai Zhang, [a] Kechun Wang, [a] Jingfeng Tian, [a] Yi Zhao, [a]Juanqin Xue [a,*]

[a] School of Chemistry and Chemical Engineering, Xi'an University of Architecture and Technology, Xi'an 710055, China

Contents

Text Sections:

Figures:

Tables:

Text S1. Analytical Methods

LC-MS/MS Analysis of Perfluoroalkyl Substances (PFAS) Concentration:

Quantification of PFAS was performed using a liquid chromatography-tandem mass spectrometry (LC-MS/MS) system (Agilent 1260 Infinity coupled with an AB Sciex Triple Quad 4500).

Liquid phase conditions: The chromatographic separation was achieved using an ACQUITY UPLC® BEH C18 column (2.1 × 50 mm, 1.7 μm) maintained at 40 °C. The mobile phase consisted of (A) 2 mM ammonium acetate in water (pH adjusted to 4.5) and (B) acetonitrile. A gradient elution program was applied as follows: initial 90% A, decreased to 5% A over 5.5 min, held for 1 min, then rapidly returned to 90% A at 6.6 min and maintained for 1.5 min for column re-equilibration. Analytes were calibrated using an internal standard method with 1/x weighted linear regression based on the relative response factors of the target analytes and their corresponding isotopically labeled standards. Data acquisition and analysis were performed using the AB Sciex Triple Quad 4500 system. All LC-MS/MS samples and standards were prepared and contained in polypropylene vials with polyethylene caps.

Mass spectrometry conditions: Ion source: Electrospray Ionization Source (ESI), negative ion mode; Capillary voltage: -4500 V; Ion source temperature: 550 ° C; Gas curtain (CUR): 35 psi; Spray gas (Gas 1): 50 psi; Auxiliary heating gas (Gas 2): 50 psi; Collision gas (CAD): Medium; Detection mode: Multiple Reaction Monitoring (MRM); Entrance voltage (EP): -10 V; Collision chamber exit voltage (CXP): -10 V. The mass-to-charge ratios (m/z), collision energies, and cluster voltages of five perfluorinated compounds and their internal standards are shown in Table S1.

This study employed the internal standard method for quantification, with an injection volume of 5 μL. The linear range of the standard curve series was 0.1, 0.2, 0.5, 1.0, 2.0, 5.0, 10.00, 20.00, and 50.00 ng/mL, and the internal standard concentration was 2.50 ng/mL. Subsequently, UPLC-MS/MS quantitative analysis was conducted to draw the standard curve. Based on the detection limit (LOD, 3 times the signal-to-noise ratio) and the quantification limit (LOQ, 10 times the signal-to-noise ratio) estimated using the method of signal-to-noise ratio at the low concentration points of the standard curve, the detection limit (LOD) and quantification limit (LOQ) were determined, along with the regression equation, correlation coefficient, detection limit, quantification limit, and matrix effect evaluation as included in Table S2.

Text S2. Synthesis of MOFs

Synthesis and Activation of MOF-808:

MOF-808 was synthesized and activated according to a previously reported method with modifications.[1] In a 1000 mL Pyrex medium bottle, $ZrOCl_2 \cdot 8H_2O$ (9.7 g, 30 mmol) and H_3BTC (2.1 g, 10 mmol) were dissolved in DMF (450 mL). An equal volume of anhydrous formic acid was then added. The mixture was placed in a preheated oven at 130 °C for 48 h. After cooling, the resulting product was collected by centrifugation and decantation. The solid was immersed in fresh DMF and dispersed via ultrasonication. This washing procedure was repeated three times per day for three days. Subsequently, the same washing protocol was performed using deionized water for three days, followed by acetone for one day. The final solid was collected by centrifugation and activated under vacuum at 140 °C for 24 h. ^{1}H NMR (400 MHz, NaOD): δ 7.73 (s, 6.00 H). Additional peaks: δ 1.51 (s, 0.54 H, DMF), δ 1.18 (s, 0.60 H, DMF), δ 0.38 (s, 0.90 H, DMF).

Synthesis and Activation of MOF-808-FR:

MOF-808-FR was prepared and activated according to another reported method with modifications.[2] Activated MOF-808 powder (5 g) was placed in a Nalgene HDPE bottle, mixed with 100 mL of 1 mM HCl solution, and shaken for 20 min. The bottle was then placed in a preheated oven at 85 °C for 120 h. During this heating period, the bottle was taken out daily, cooled, centrifuged, and the supernatant was decanted and replaced with an equal volume of fresh HCl solution; this replacement was performed three times per day. After heating, the sample was cooled, centrifuged, and washed. The resulting solid was immersed in deionized water and dispersed via ultrasonication; this procedure was repeated three times per day for three days, followed by the same protocol with acetone for one day. The solid was finally activated under vacuum at 140 °C for 24 h. ^{1}H NMR (400 MHz, NaOD): δ 7.73 (s, 6.00 H). Additional peaks: δ 1.51 (s, 0.54 H, DMF), δ 1.18 (s, 0.60 H, DMF), δ 0.38 (s, 0.90 H, DMF).

Synthesis and Activation of MOF-808-Gly:

In a 250 mL Pyrex medium bottle, activated MOF-808-FR powder (1 g) was combined with an aqueous glycine solution (3 mM, 200 mL) and shaken for 20 min. The mixture was heated in a preheated oven at 85 °C for 72 h. During heating, the supernatant was replaced with fresh glycine solution twice daily. After heating, the sample was cooled, centrifuged, and decanted. The

resulting solid was immersed in deionized water and dispersed via ultrasonication; this procedure was repeated three times per day for three days, followed by the same protocol with acetone for one day. The solid was sequentially dried under vacuum at 30 °C for 3 h, 60 °C for 2 h, and 140 °C for 20 h to yield activated MOF-808-Gly. ^{1}H NMR (400 MHz, NaOD): δ 7.73 (s, 6.00 H), δ 2.38 (s, 8.34 H). Additional peaks: δ 1.51 (s, 0.54 H, DMF), δ 1.18 (s, 0.60 H, DMF), δ 0.38 (s, 0.90 H, DMF).

Synthesis and Activation of MOF-808-Ala:

In a 250 mL Pyrex medium bottle, activated MOF-808-FR powder (1 g) was combined with an aqueous DL-alanine solution (1.7 mM, 200 mL) and shaken for 20 min. The mixture was heated in a preheated oven at 85 °C for 72 h. During heating, the supernatant was replaced with fresh DL-alanine solution twice daily. After heating, the sample was cooled, centrifuged, and decanted. The resulting solid was immersed in deionized water and dispersed via ultrasonication; this procedure was repeated three times per day for three days, followed by the same protocol with acetone for one day. The solid was sequentially dried under vacuum at 30 °C for 3 h, 60 °C for 2 h, and 140 °C for 20 h to yield activated MOF-808-Ala. ^{1}H NMR (400 MHz, NaOD): δ 7.73 (s, 6.00 H), δ 2.55 (s, 2.24 H), δ 0.46 (s, 12.62 H). Additional peaks: δ 1.51 (s, 0.54 H, DMF), δ 1.18 (s, 0.60 H, DMF), δ 0.38 (s, 0.90 H, DMF).

Synthesis and Activation of MOF-808-Dap:

For the synthesis of MOF-808-Dap, the concentration of the 2,3-diaminopropanoic acid solution was screened (0.05 M, 0.10 M, and 0.15 M) by reacting with MOF-808-FR (1 g) in a 250 mL Pyrex medium bottle. The mixture was heated in a preheated oven at 85 °C for 72 h. During heating, the supernatant was replaced with fresh 2,3-diaminopropanoic acid solution twice daily. After heating, the sample was cooled, centrifuged, and decanted. The resulting solid was immersed in deionized water and dispersed via ultrasonication; this procedure was repeated three times per day for three days, followed by the same protocol with acetone for one day. The solid was sequentially dried under vacuum at 30 °C for 3 h, 60 °C for 2 h, and 140 °C for 20 h. The optimal condition (0.05 M) was selected to maximize the degree of functionalization while maintaining crystallinity, yielding activated MOF-808-Dap. ^{1}H NMR (400 MHz, NaOD): δ 7.73 (s, 6.00 H), δ 2.56 (s, 7.02 H), δ 2.05 (s, 5.39 H), δ 0.43 (s, 3.39 H), δ 0.27 (s, 4.72 H). Additional peaks: δ 1.51 (s, 0.54 H, DMF), δ 1.18 (s, 0.60 H, DMF), δ 0.38 (s, 0.90 H, DMF).

Synthesis and Activation of MOF-808-TFA:

In a 250 mL Pyrex medium bottle, activated MOF-808 powder (1 g) was combined with trifluoroacetic acid (1860 µL) and DMF (100 mL), shaken for 20 min, and then stirred in an oil bath at 85 °C for 24 h. After cooling, the sample was centrifuged and decanted. The resulting solid was immersed in methanol and dispersed via ultrasonication; this procedure was repeated three times per day for three days, followed by the same protocol with acetone for one day. The solid was activated under vacuum at 140 °C for 24 h. ^{1}H NMR (400 MHz, NaOD): δ 7.73 (s, 6.00 H). Additional peaks: δ 1.51 (s, 0.54 H, DMF), δ 1.18 (s, 0.60 H, DMF), δ 0.38 (s, 0.90 H, DMF). ^{19}F NMR: δ -75.21 (TFA), -76.00 (TFE standard).

Synthesis and Activation of MOF-808-TFPA:

In a 250 mL Pyrex medium bottle, activated MOF-808 powder (1 g) was combined with 3,3,3-trifluoropropanoic acid (2210 µL) and DMF (100 mL), shaken for 20 min, and then stirred in an oil bath at 85 °C for 24 h. After cooling, the sample was centrifuged and decanted. The resulting solid was immersed in methanol and dispersed via ultrasonication; this procedure was repeated three times per day for three days, followed by the same protocol with acetone for one day. The solid was activated under vacuum at 140 °C for 24 h. ^{1}H NMR (400 MHz, NaOD): δ 7.73 (s, 6.00 H). Additional peaks: δ 1.51 (s, 0.54 H, DMF), δ 1.18 (s, 0.60 H, DMF), δ 0.38 (s, 0.90 H, DMF). ^{19}F NMR: δ -147.63 (TFPA), -76.00 (TFE standard).

Synthesis and Activation of MOF-808-PFPA:

In a 250 mL Pyrex medium bottle, activated MOF-808 powder (1 g) was combined with pentafluoropropanoic acid (2270 µL) and DMF (100 mL), shaken for 20 min, and then stirred in an oil bath at 85 °C for 24 h. After cooling, the sample was centrifuged and decanted. The resulting solid was immersed in methanol and dispersed via ultrasonication; this procedure was repeated three times per day for three days, followed by the same protocol with acetone for one day. The solid was activated under vacuum at 140 °C for 24 h. ^{1}H NMR (400 MHz, NaOD): δ 7.73 (s, 6.00 H). Additional peaks: δ 1.51 (s, 0.54 H, DMF), δ 1.18 (s, 0.60 H, DMF), δ 0.38 (s, 0.90 H, DMF). ^{19}F NMR: δ -20.97 (PFPA), δ -83.24 (PFPA), -76.00 (TFE standard).

Synthesis and Activation of MOF-808-TFMA:

For the synthesis of MOF-808-TFMA, the concentration of the 3,3,3-trifluoro-DL-alanine aqueous solution was screened (0.05 M, 0.10 M, and 0.15 M) by reacting with MOF-808-FR (1 g) in a 250 mL Pyrex medium bottle. The mixture was heated in a preheated oven at 85 °C for 72 h. During

heating, the supernatant was replaced with fresh 3,3,3-trifluoro-DL-alanine solution twice daily. After heating, the sample was cooled, centrifuged, and decanted. The resulting solid was immersed in deionized water and dispersed via ultrasonication; this procedure was repeated three times per day for three days, followed by the same protocol with acetone for one day. The solid was sequentially dried under vacuum at 30 °C for 3 h, 60 °C for 2 h, and 140 °C for 20 h. The optimal condition (0.05 M) was selected to maximize the degree of functionalization while maintaining crystallinity, yielding activated MOF-808-TFMA. ^{1}H NMR (400 MHz, NaOD): δ 7.73 (s, 6.00 H), δ 2.75 (s, 2.48 H), δ 2.40 (s, 2.77 H). Additional peaks: δ 1.51 (s, 0.54 H, DMF), δ 1.18 (s, 0.60 H, DMF), δ 0.38 (s, 0.90 H, DMF). ^{19}F NMR: δ -148.05 (TFMA), -76.00 (TFE standard).

Text S3. Adsorption Experiments

Analysis of Solution after Adsorption:

The adsorption capacity of the adsorbent was determined using Equation S1:

$$Q_t = \frac{(C_0 - C_t)}{m} \cdot \mathrm{V} \quad (1)$$

where Q_t (mg/g) is the adsorption capacity of the MOF at a given time t (min), C_0 and C_t are the contaminant concentrations (mg/L) before and after the experiment, respectively, V is the volume of the PFAS solution (mL), and m is the mass of the adsorbent used (g).

For trace PFAS concentrations, the removal efficiency of the adsorbent was determined using Equation S2:

$$\text{Efficiency}(\%) = \frac{C_0 - C_t}{C_0} \cdot 100\% \quad (2)$$

where C_0 and C_t are the contaminant concentrations (mg/L) before and after the experiment, respectively.

The loss of target PFAS adsorbed onto the container is calculated by the difference in PFAS concentration in the water sample before and after the experimental step (oscillation). The container removal rate (R, %) is determined using the formula S3:

$$R(\%) = \frac{C_x}{C_0} \cdot 100\% \quad (3)$$

$$RSD\ (\%, n=3) = \frac{standard\ deviation\ (SD)}{mean\ value\ (Mean)} \cdot 100\% \quad (4)$$

where C_0 represents the initial concentration, while C_x represents the concentration after oscillation (μg/L). The data is derived from the blank experiments of spiked recovery conducted on the same batch and with the same concentration (Table S8).

Adsorption Kinetics and Isotherms

Following the initial assessment of PFAS adsorption performance, selected high-performance materials were subjected to adsorption kinetics tests to determine the equilibrium time required for removal, as well as adsorption isotherms. The initial concentrations for the adsorption kinetics study were the same as those in the preliminary adsorption experiments. Samples were taken at 1, 5, 10, 20, 30, 60, 90, 180, 360, and 720 minutes, and the data were fitted using the pseudo-second-order kinetic model (Equation S3). Adsorption isotherms were typically generated by adding MOFs to polyethylene bottles containing varying concentrations of the contaminant (0–800 ppm). After 1440 minutes, the adsorption isotherms were fitted using the Langmuir (Equation S4) and Freundlich (Equation S5) models. These mixtures were placed in a constant-temperature shaker and adsorbed for 1440 minutes under different temperature conditions (288.15 K, 298.15 K, and 303.15 K). The final PFAS concentrations were measured by LC-MS/MS.

Pseudo-second-order kinetic model:

$$Q_t = \frac{k_2\, Q_e^2 t}{1 + k_2 Q_e t} \quad (5)$$

where t is the adsorption time (min), k_2 (g·mg⁻¹·min⁻¹) is the pseudo-second-order adsorption rate constant, and Q_t and Q_e are the adsorption capacities (mg/g) at time t and at equilibrium, respectively.

Langmuir model:

$$Q_e = \frac{(Q_m \times k_L \times C_e)}{1 + k_L \times C_e} \quad (6)$$

where Q_e (mg·g⁻¹) is the adsorption capacity at equilibrium, Q_m (mg·g⁻¹) is the maximum adsorption capacity of the adsorbent, C_e (mg·L⁻¹) is the contaminant concentration at adsorption equilibrium, and k_L (L·mg⁻¹) is the Langmuir equilibrium constant.

Freundlich model:

$$Qe = C_e^{1/n} \times k_f \quad (7)$$

where Q_e (mg·g⁻¹) is the adsorption capacity at equilibrium, C_e (mg·L⁻¹) is the residual concentration at equilibrium, k_F (mg·g⁻¹·(L·mg⁻¹)¹/ⁿ) is the Freundlich constant, and n is an indicator of adsorption intensity.

Thermodynamic Parameters

Thermodynamic parameters, including the standard Gibbs free energy change (ΔG°, kJ/mol), standard enthalpy change (ΔH°, kJ/mol), and standard entropy change (ΔS°, J/(mol·K)), were derived using Equations S6–S9.

$$\Delta G^0 = \Delta H^0 - T\Delta S^0 \quad (8)$$

$$\Delta G^0 = - RTlnK^0 \quad (9)$$

$$K^0 = K_L[\frac{L}{mg}] \times C_{ref} \times Mw \quad (10)$$

$$lnK^0 = \frac{\Delta S^0}{R} - \frac{\Delta H^0}{RT} \quad (11)$$

Here, R (8.314 J/(K·mol)) is the universal gas constant, *T* (K) is the absolute temperature, K^0 is the dimensionless equilibrium constant, K_L (L/mg) is the adsorption equilibrium constant obtained by fitting the Langmuir model, M_w is the molecular weight of the solute, and C_{ref} is the solute concentration in the reference state for the dissolved solute ($C_{\text{ref}} = 1$ mol/L).

Regeneration and Cycling Experiments

Regeneration studies were conducted by adding 10 mg of MOFs to 25 mL of PFAS solution, followed by shaking in an incubator shaker at 180 rpm and room temperature. After centrifugation at room temperature, the supernatant was collected and analyzed for PFAS concentration. The collected supernatants were combined and filtered through a 0.25 μm nylon membrane. The remaining saturated solid MOFs were placed in 20 mL of regeneration solvent, subjected to ultrasonication at room temperature, and then shaken for 30 minutes. Finally, the regeneration solvent containing the adsorbent was collected via centrifugation at room temperature and filtered through a 0.25 μm nylon membrane for reuse. Prior to the next adsorption cycle, the

regenerated adsorbent was vacuum-dried. All experiments were performed in triplicate, and the average values are reported.

Text S4. Computational Methods

All simulations related to Density Functional Theory (DFT) were performed using the Materials Studio (MS) 2020 software package. In this study, density functional theory (DFT) calculations focusing on the adsorption of PFOA, PFHxA, and PFBA were performed primarily for MOF-808-Ala, -PFPA, and -TFMA, which are functionalized derivatives of the parent MOF-808. Due to the excessively large unit cell of MOF-808, which precludes the evaluation of all possible adsorption configurations, a cluster model composed of two Zr secondary building units (SBUs) connected by a single benzene-1,3,5-tricarboxylate linker was employed to conserve computational resources. Geometry optimizations were carried out using the Forcite module. The adsorption energy of PFAS on the MOF was calculated as follows:

$$E_{adsorption} = E_{MOF/PFAS} - E_{MOF} - E_{PFAS} \quad (13)$$

where E_{ads}, $E_{MOF/PFAS}$, E_{MOF}, and E_{PFAS} represent the energy of the adsorbed system, the energy of the adsorbent before adsorption, and the energy of the adsorbate before adsorption, respectively. A more negative value of E_{ads} indicates a stronger binding between the adsorbent and adsorbate. For each adsorption site, two or more orientations of the PFAS molecule were considered to evaluate the effect of different orientations on PFAS capture. Finally, the electrostatic potential (ESP) surfaces of the computational models were visualized to understand the electron density distribution.

Figure S1. ^{1}H NMR spectrum (400 MHz) of pre-screened MOF-808-Dap and MOF-808-TFMA digested in NaOD.

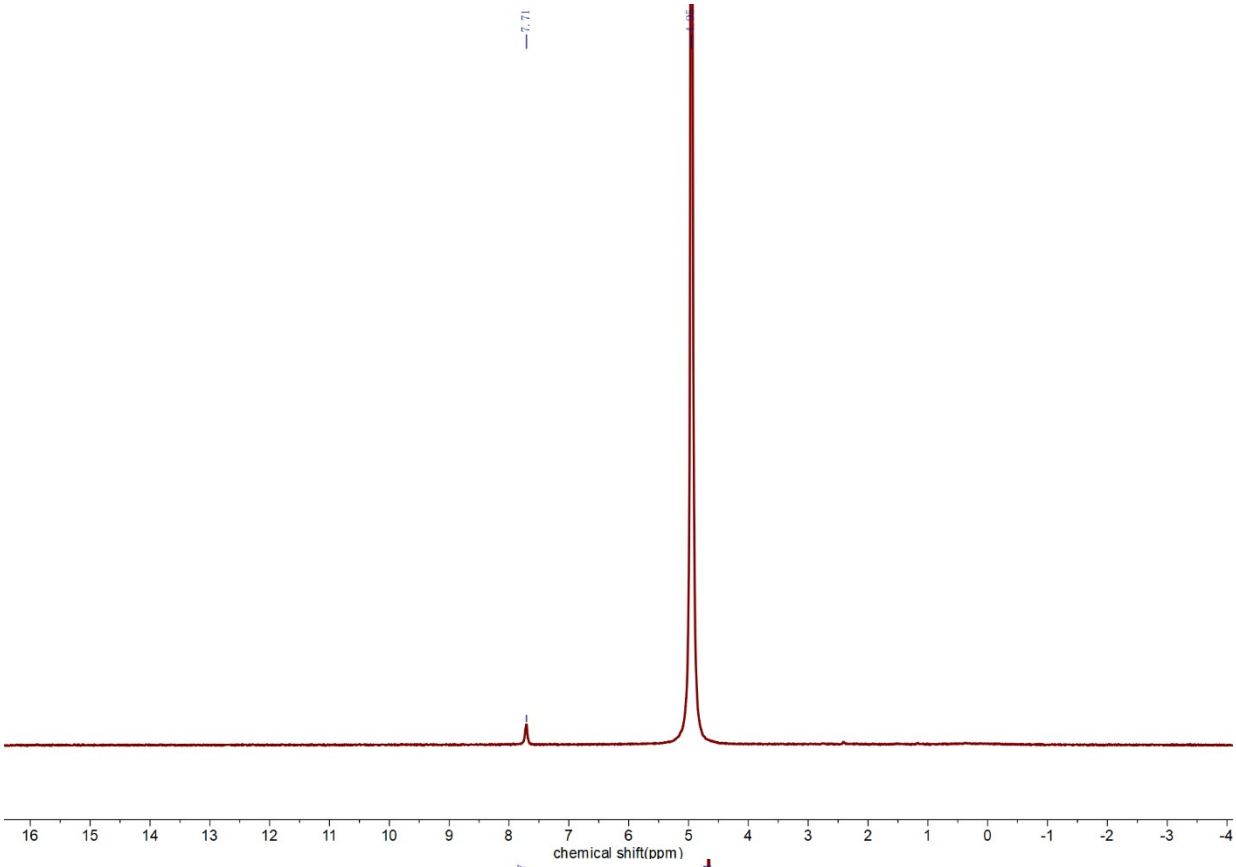

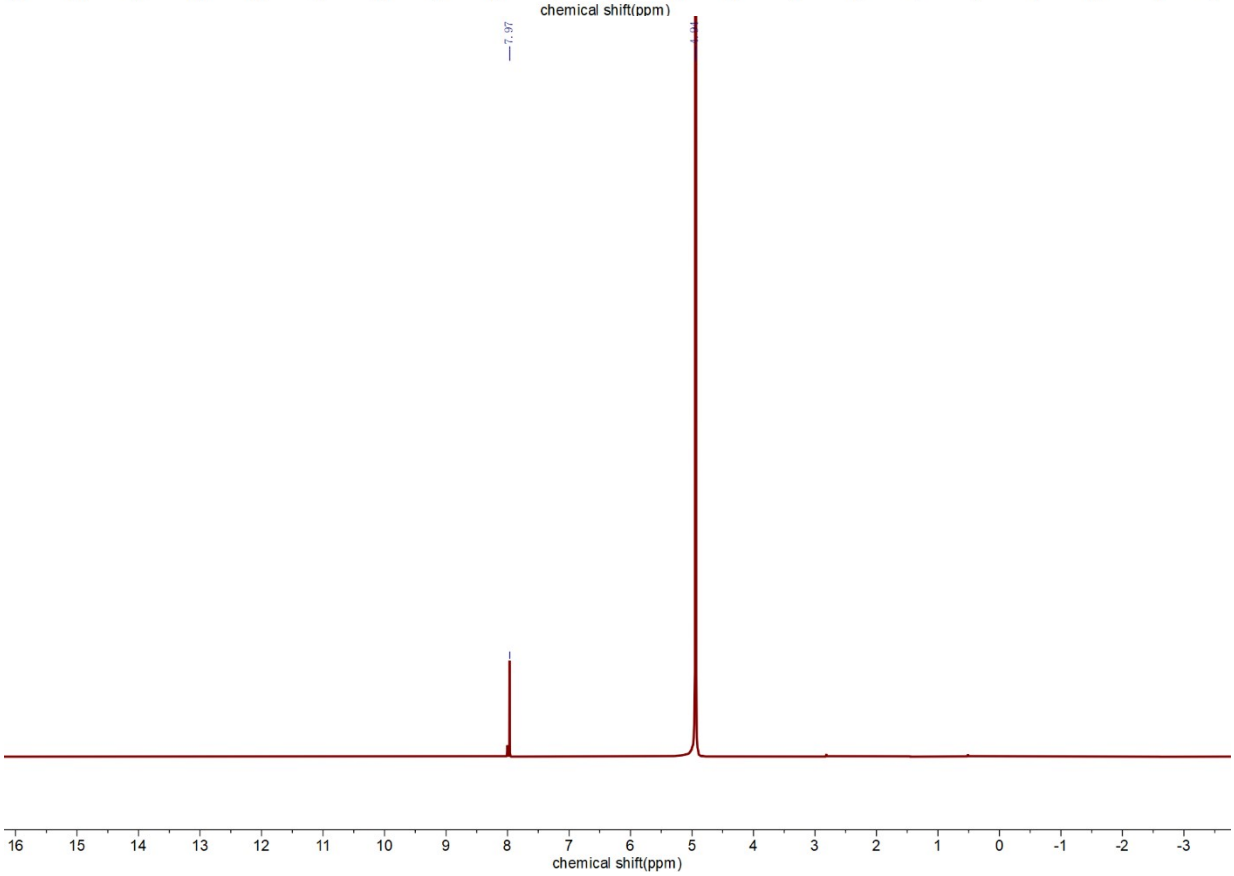

Figure S2. ^{1}H NMR spectrum (400 MHz) of activated MOF-808 digested in NaOD. Minor impurities are observed and attributed to residual solvents.

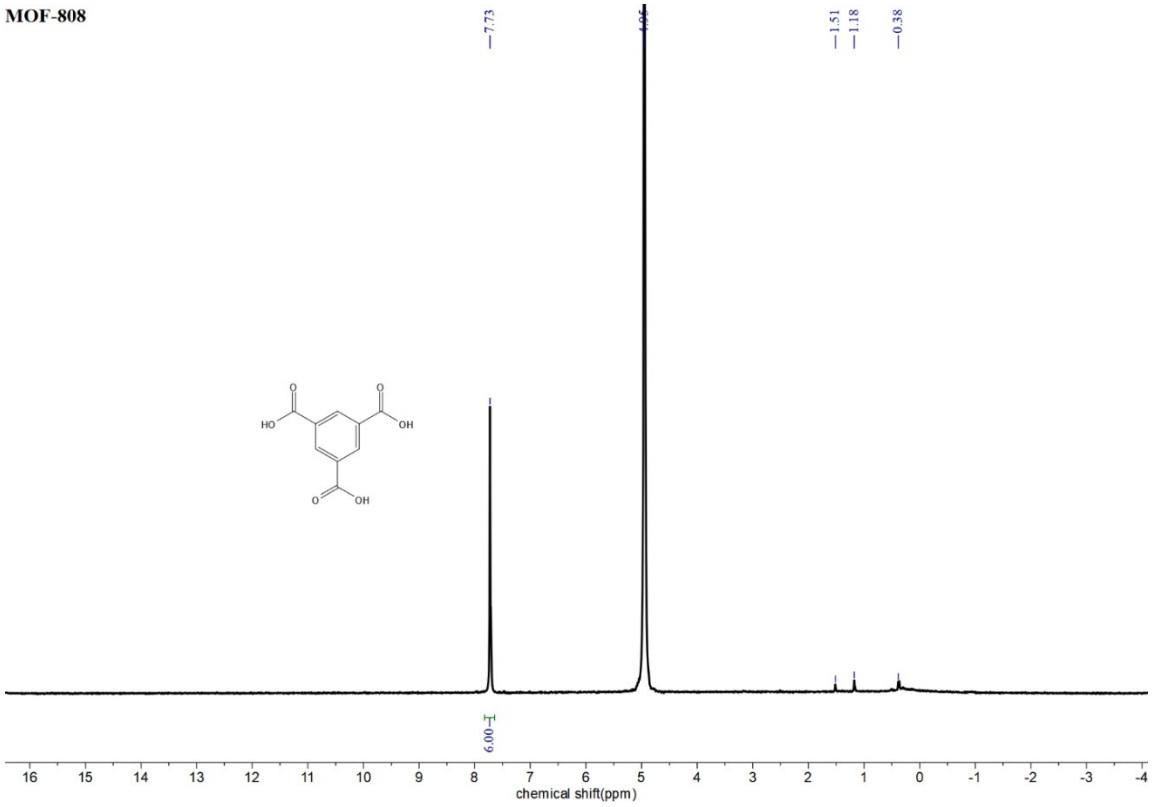

Figure S3. ^{1}H NMR spectrum (400 MHz) of activated MOF-808-FR digested in NaOD. Minor impurities are observed and attributed to residual solvents.

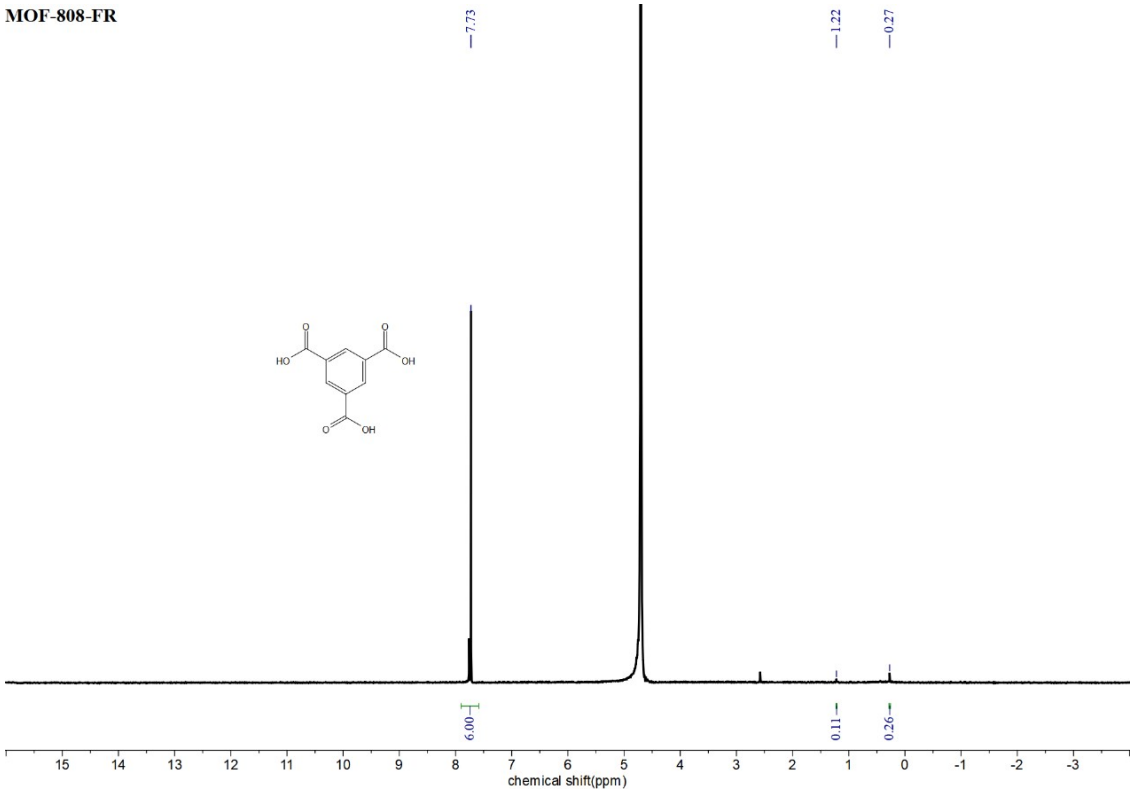

Figure S4. [1]H NMR spectrum (400 MHz) of activated MOF-808-Gly digested in NaOD. Minor impurities are observed and attributed to residual solvents.

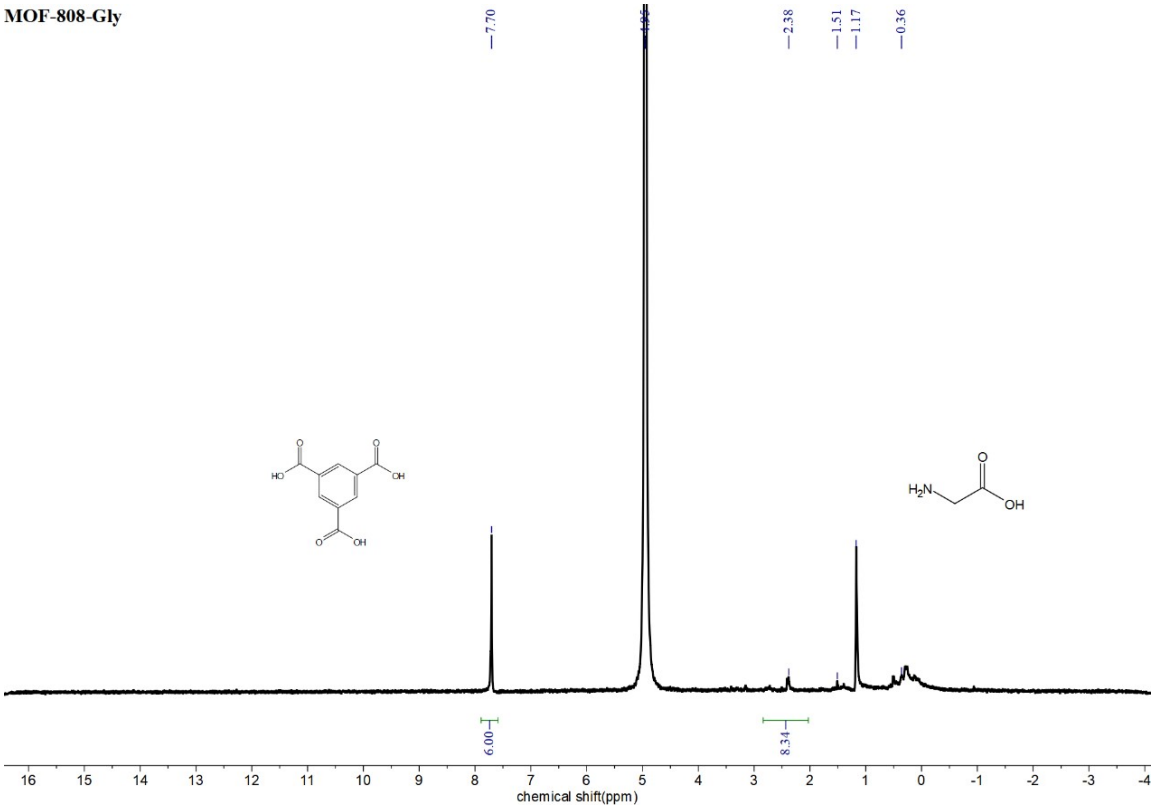

Figure S5. [1]H NMR spectrum (400 MHz) of activated MOF-808-Ala digested in NaOD. Minor impurities are observed and attributed to residual solvents.

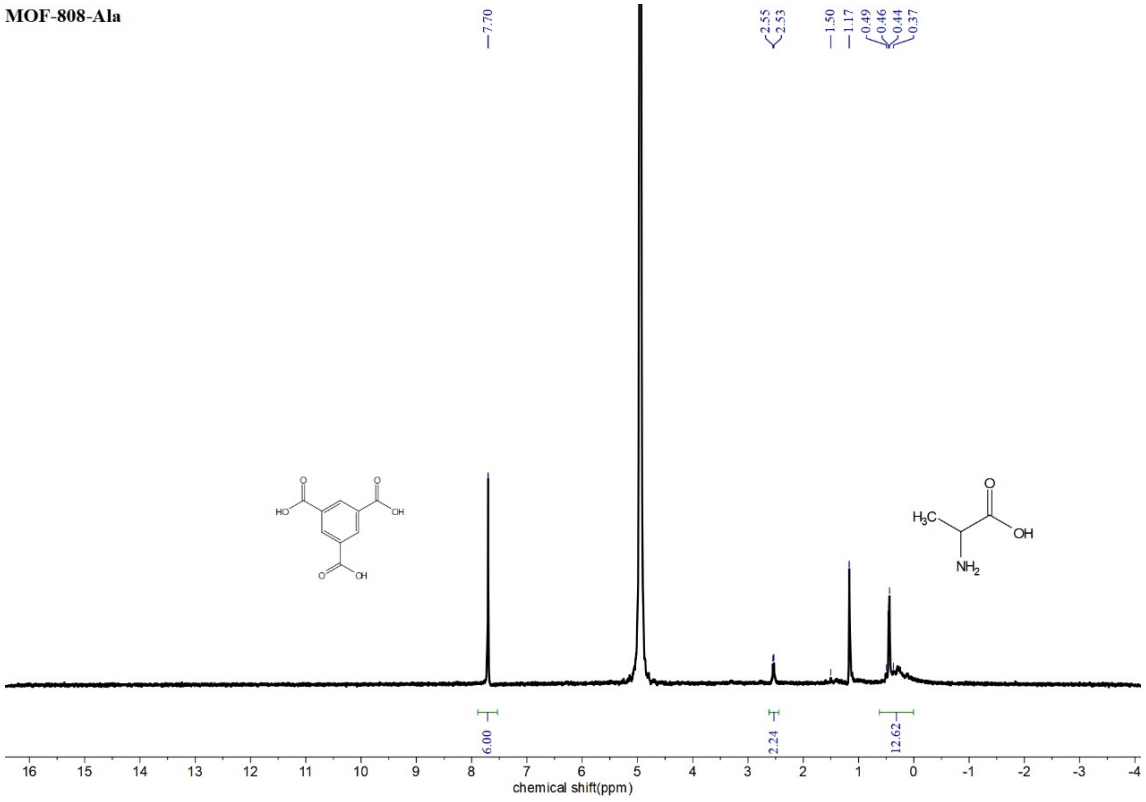

Figure S6. ^{1}H NMR spectrum (400 MHz) of activated MOF-808-Dap digested in NaOD. Minor impurities are observed and attributed to residual solvents.

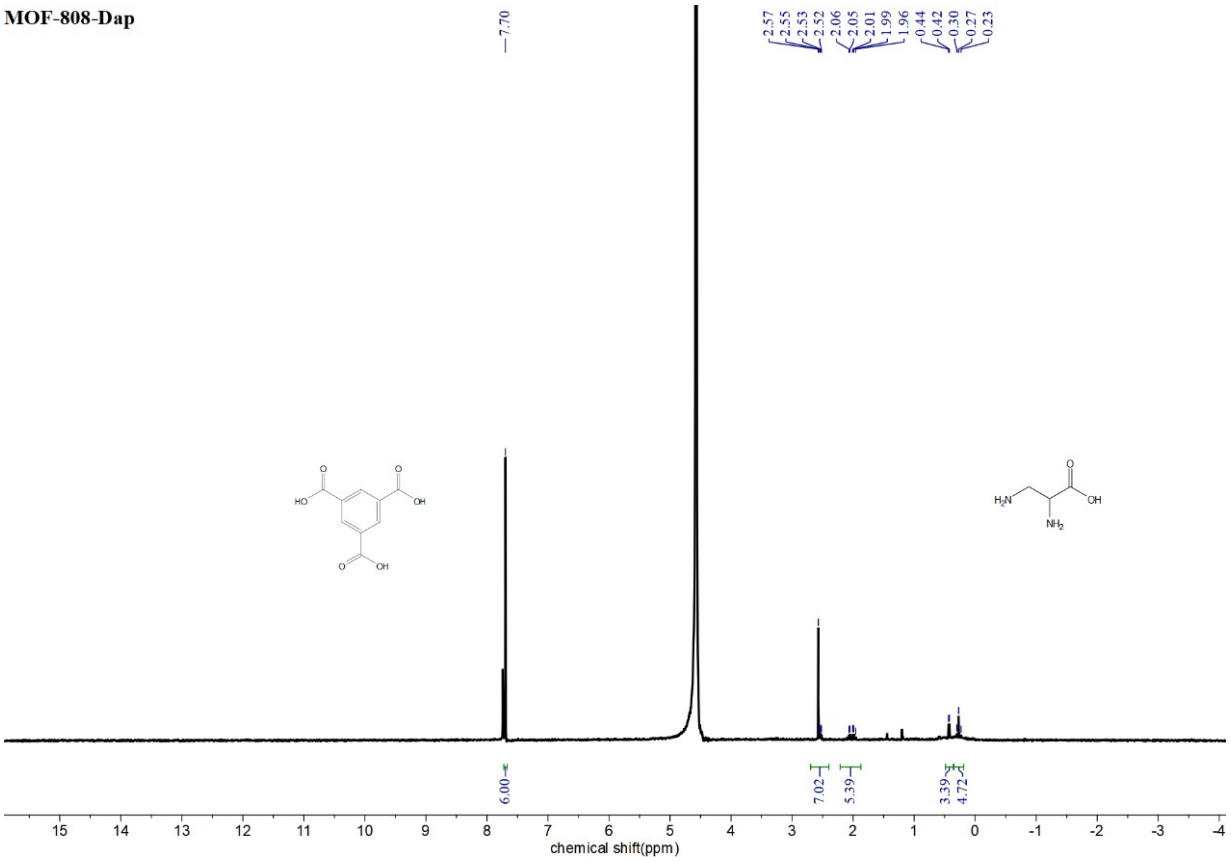

Figure S7. ^{1}H NMR (top, 400 MHz) and ^{19}F NMR (bottom, 600 MHz, with TFE as internal standard) spectra of activated MOF-808-TFA digested in NaOD. Minor impurities are observed and attributed to residual solvents.

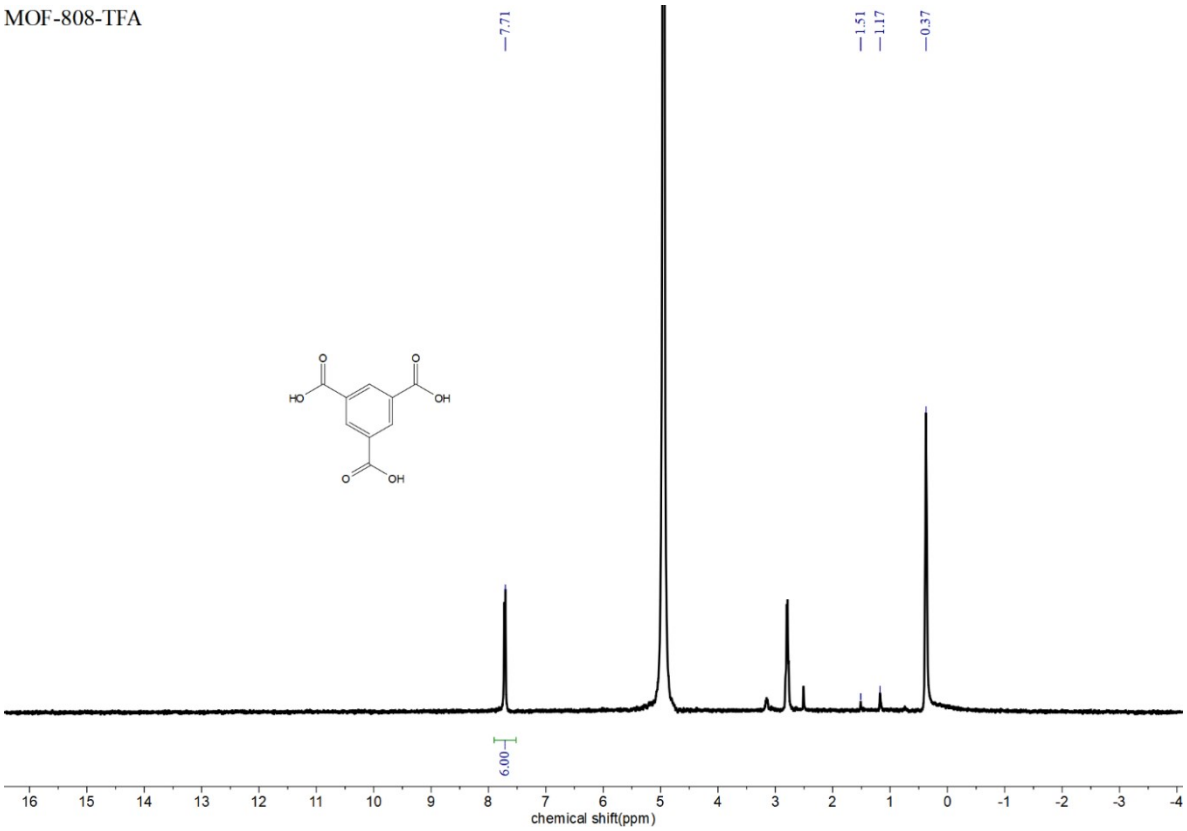

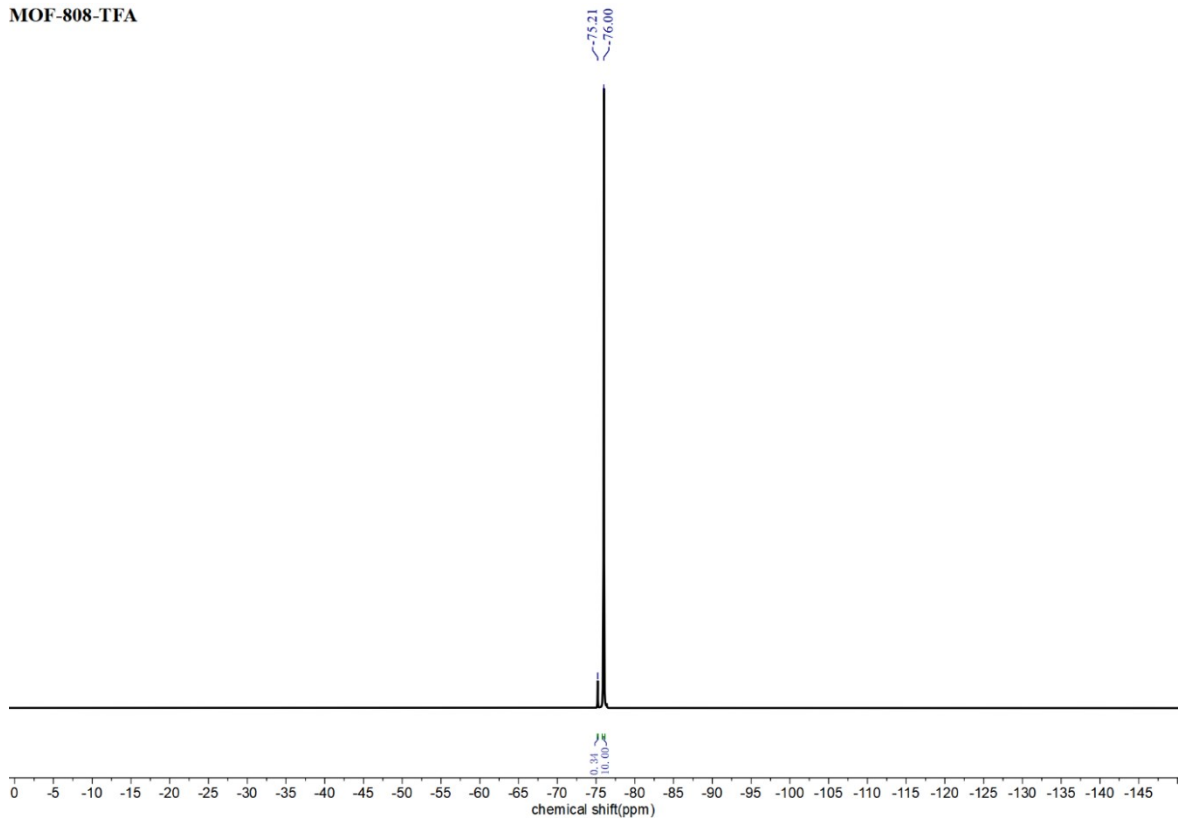

Figure S8. ^{1}H NMR (top, 400 MHz) and ^{19}F NMR (bottom, 600 MHz, with TFE as internal standard) spectra of activated MOF-808-TFPA digested in NaOD. Minor impurities are observed and attributed to residual solvents.

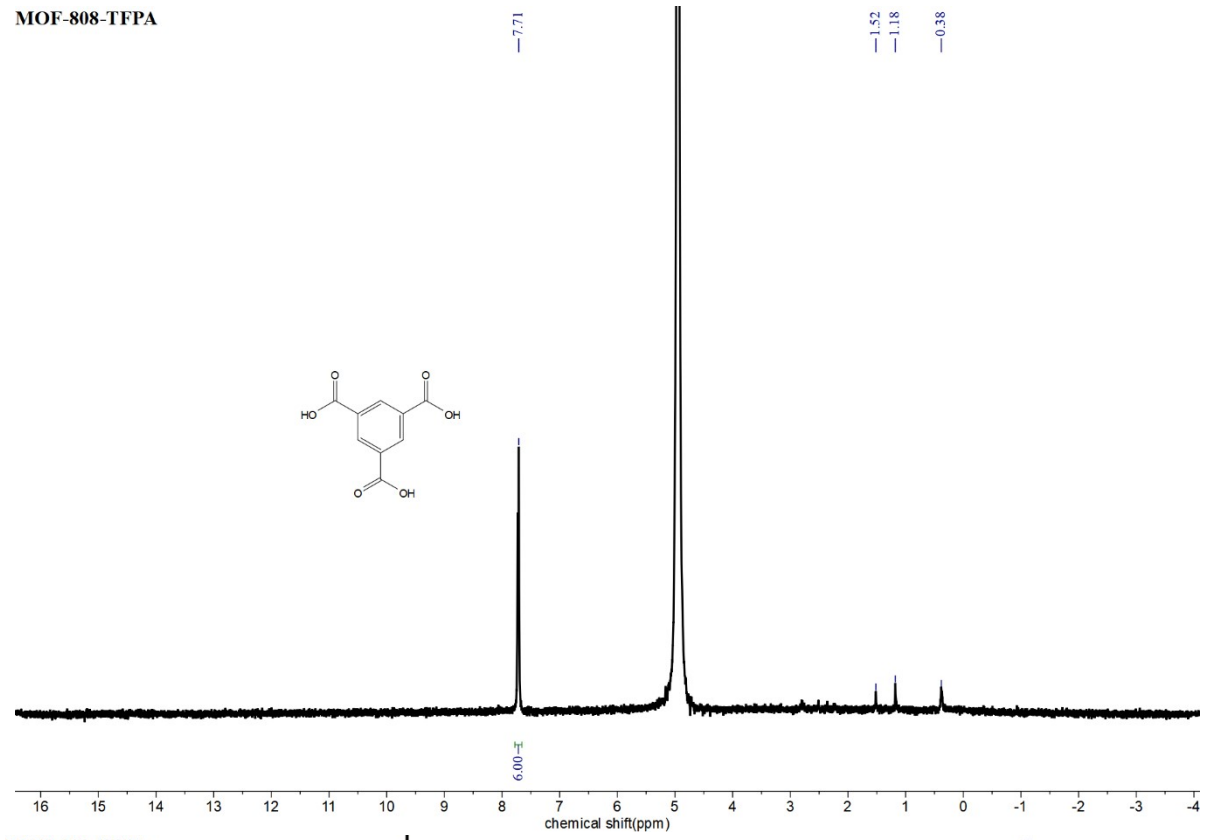

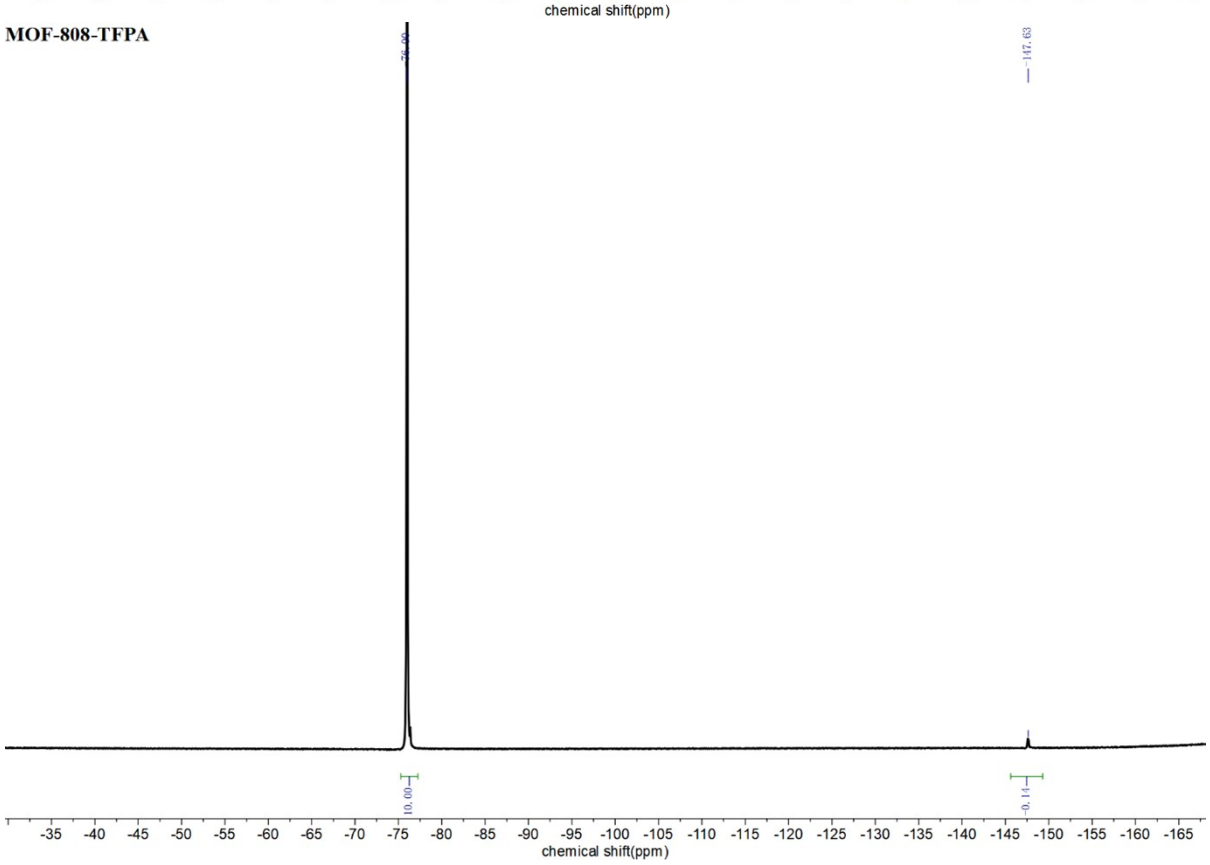

Figure S9. ^{1}H NMR (top, 400 MHz) and ^{19}F NMR (bottom, 600 MHz, with TFE as internal standard) spectra of activated MOF-808-PFPA digested in NaOD. Minor impurities are observed and attributed to residual solvents.

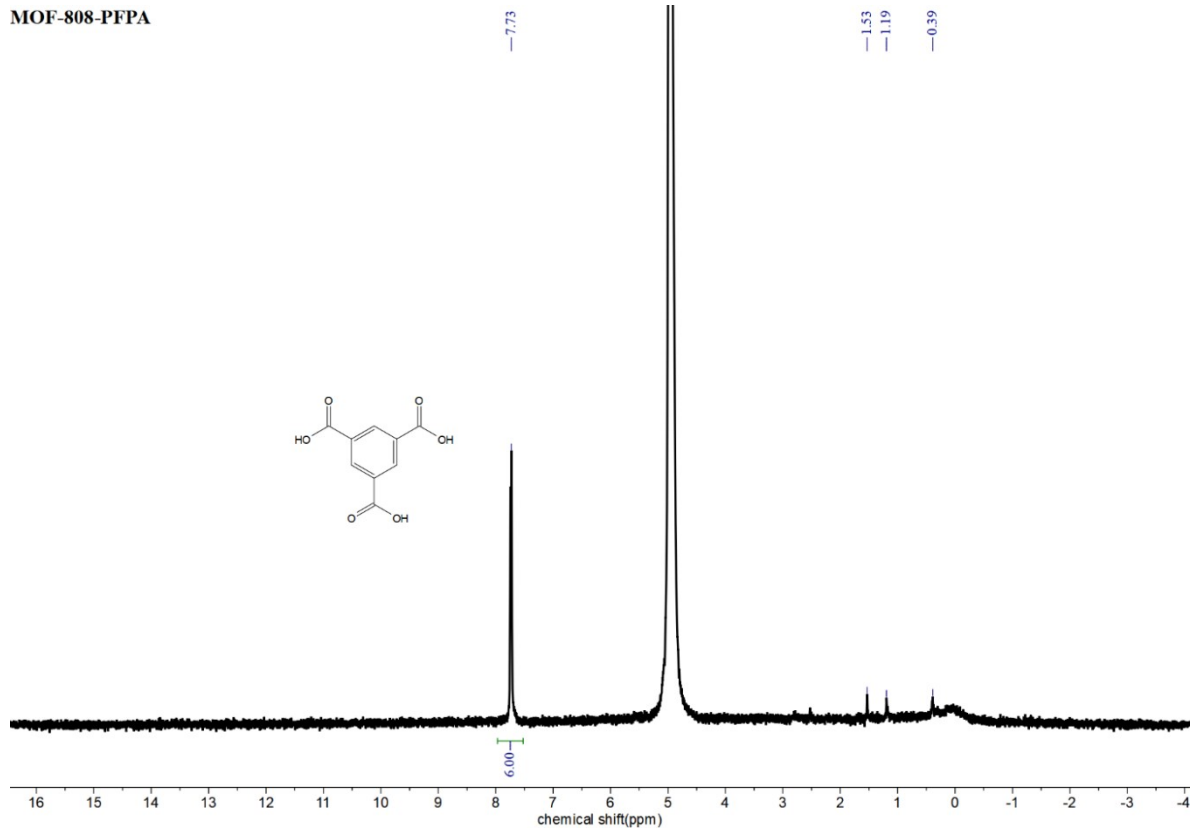

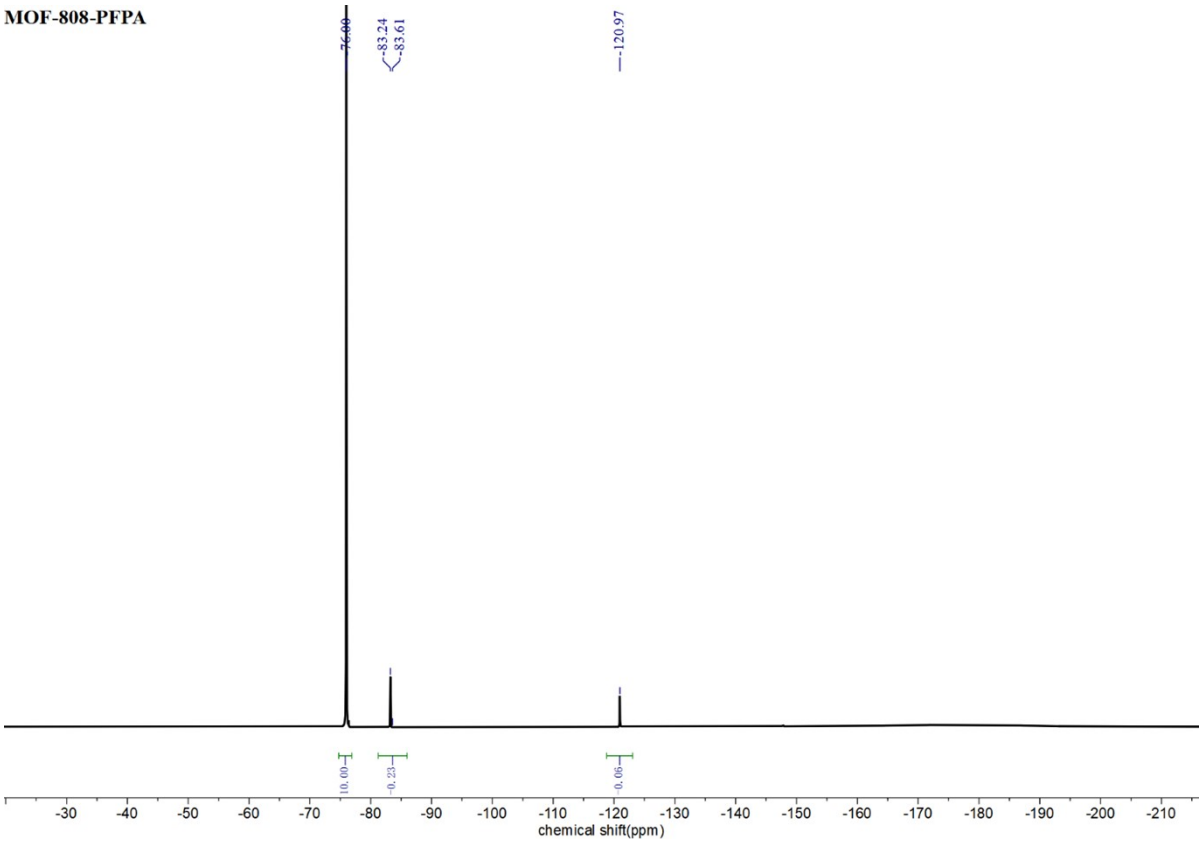

Figure S10. ^{1}H NMR (top, 400 MHz) and ^{19}F NMR (bottom, 600 MHz, with TFE as internal standard) spectra of activated MOF-808-TFMA digested in NaOD. Minor impurities are observed and attributed to residual solvents.

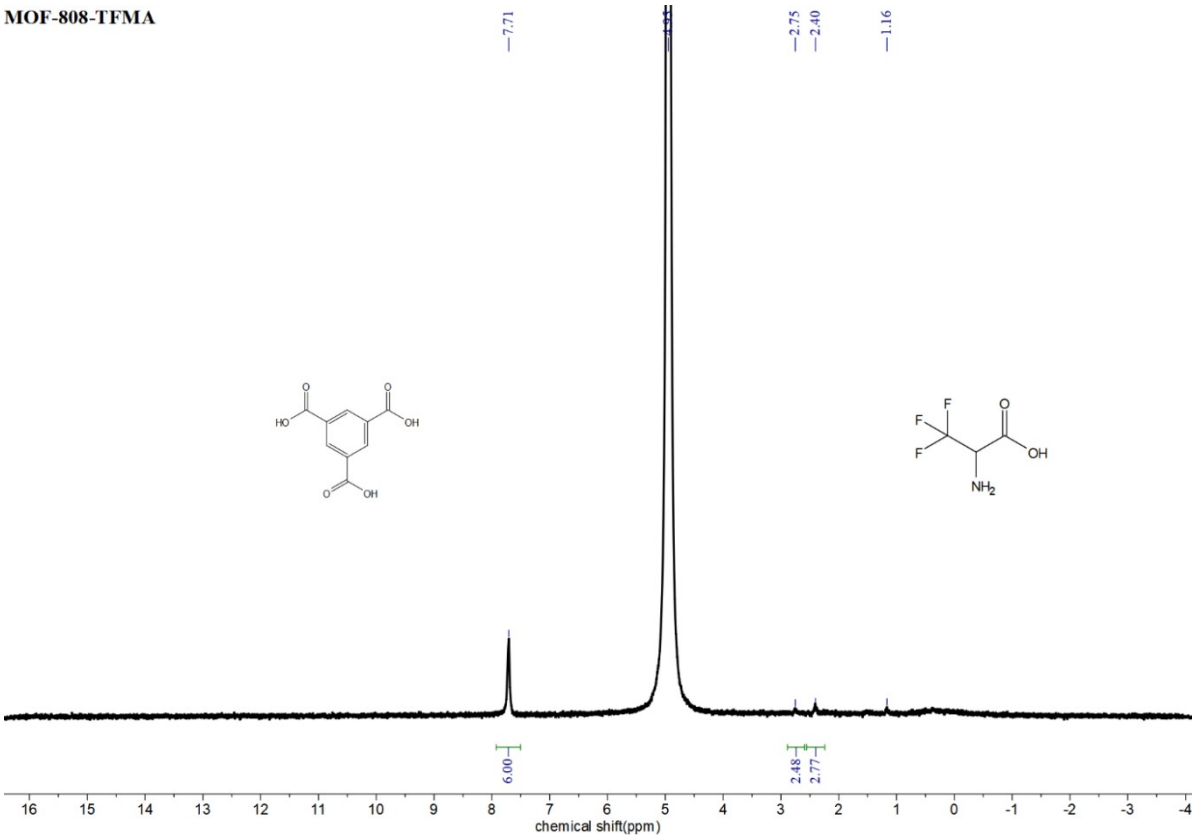

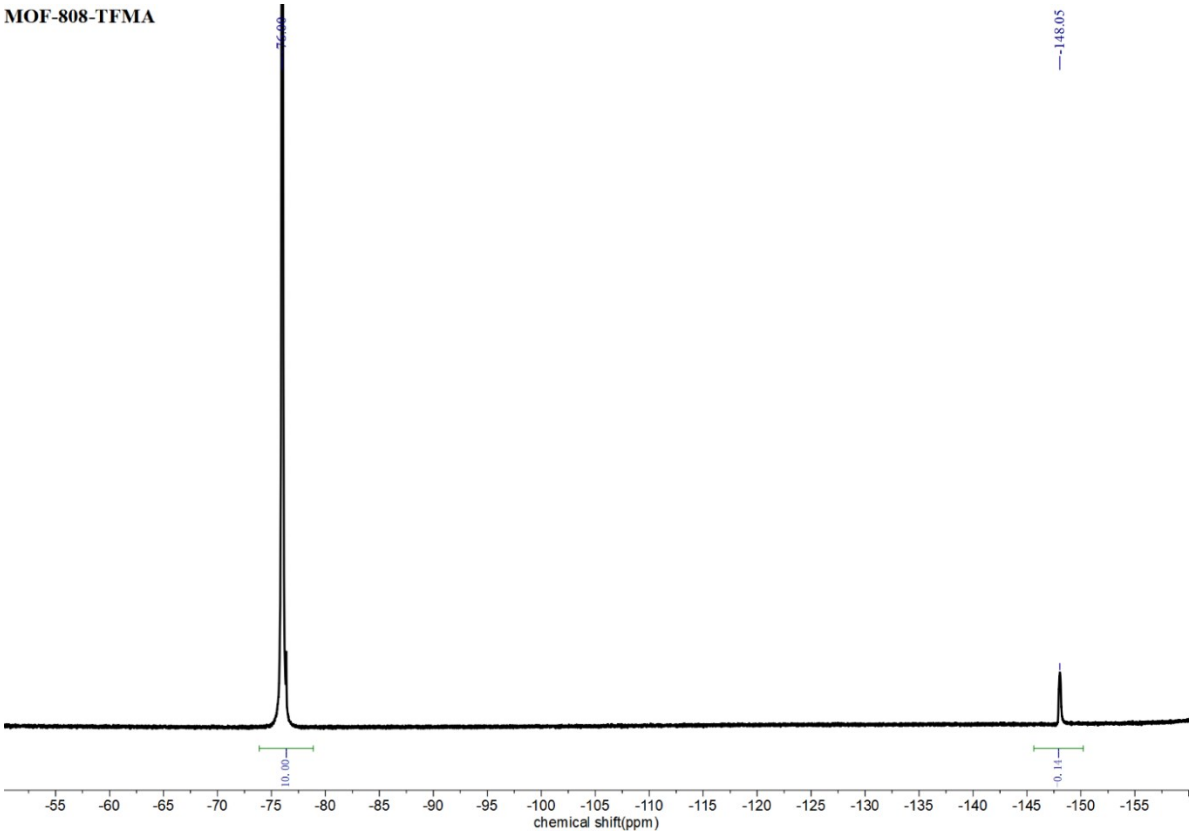

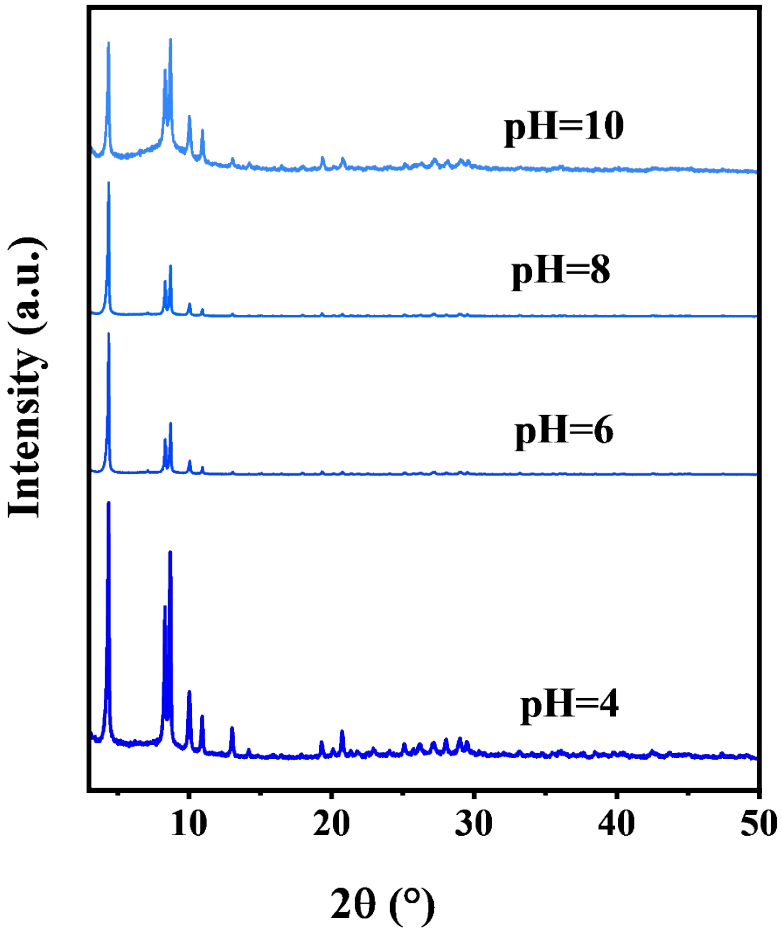

Figure S11. PXRD spectra of MOF-808-TFMA exposed in water solutions of different pH values

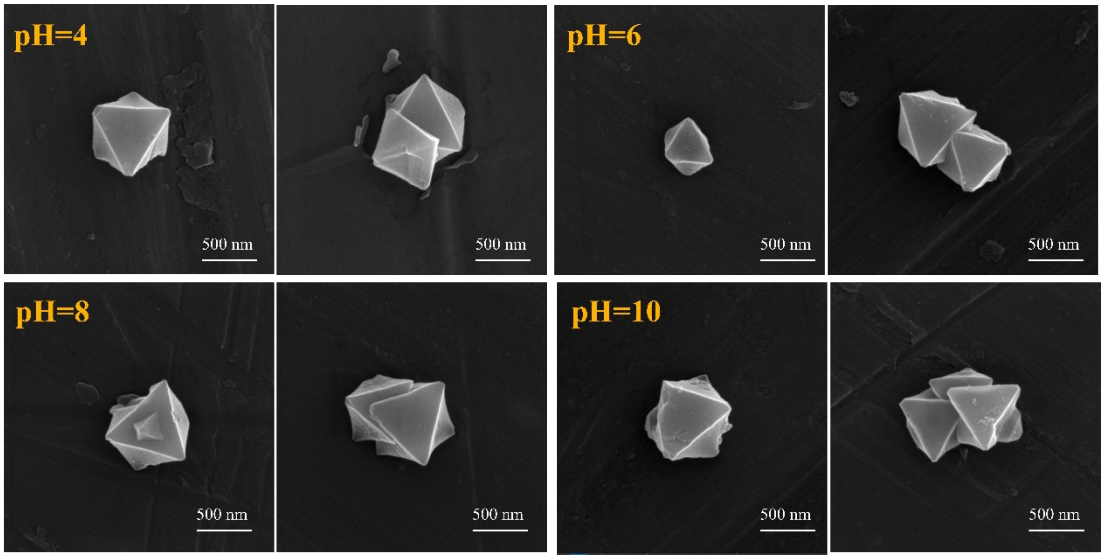

Figure S12. SEM spectra of MOF-808-TFMA exposed in water solutions of different pH values

Figure S13. Thermogravimetric analysis (TGA) of pristine and functionalized MOF-808 samples.

a

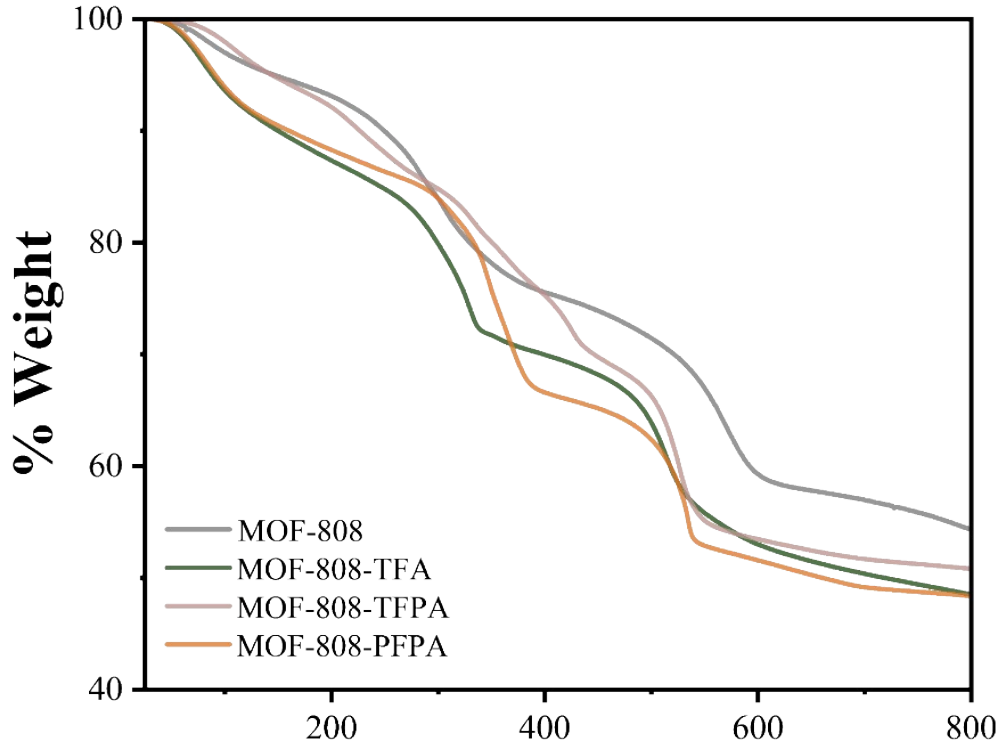
100
80
60
40
% Weight
200
400
600
800
Temperature(°C)
MOF-808
MOF-808-TFA
MOF-808-TFPA
MOF-808-PFPA

b

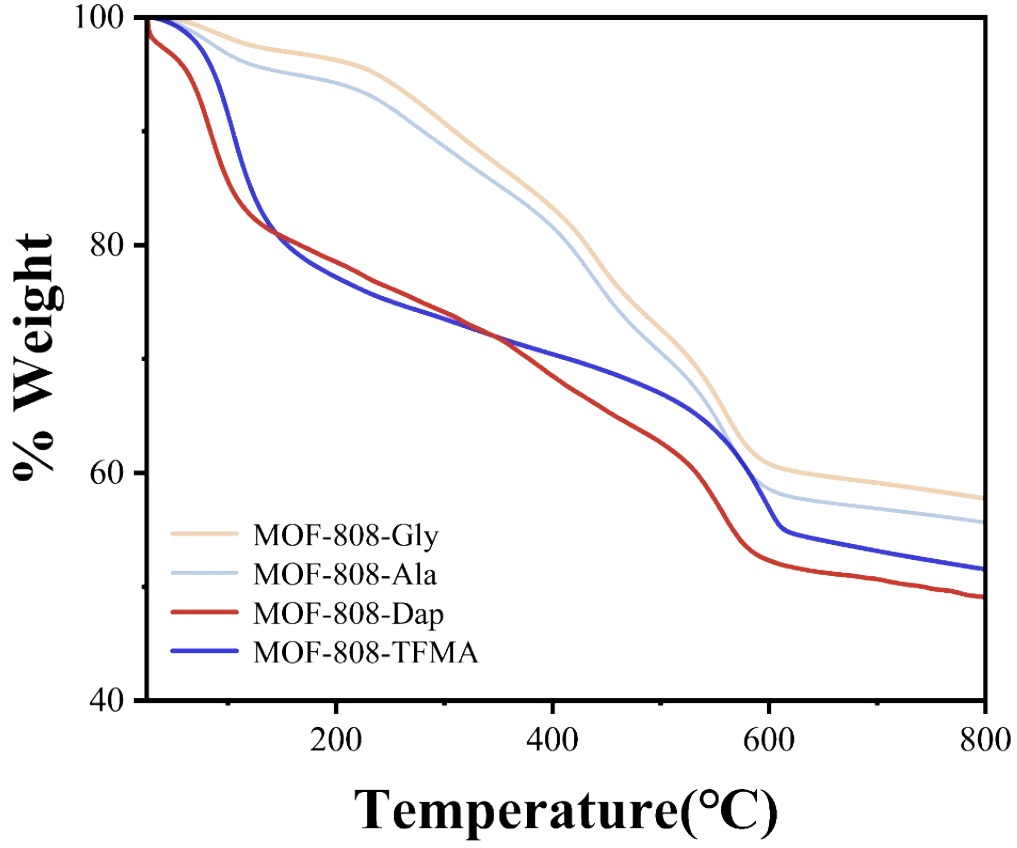
100
80
60
40
% Weight
200
400
600
800
Temperature(°C)
MOF-808-Gly
MOF-808-Ala
MOF-808-Dap
MOF-808-TFMA

Figure S14. SEM images of (a) MOF-808-TFA, (b) MOF-808-TFPA, (c) MOF-808-Gly, and (d) MOF-808-Dap.

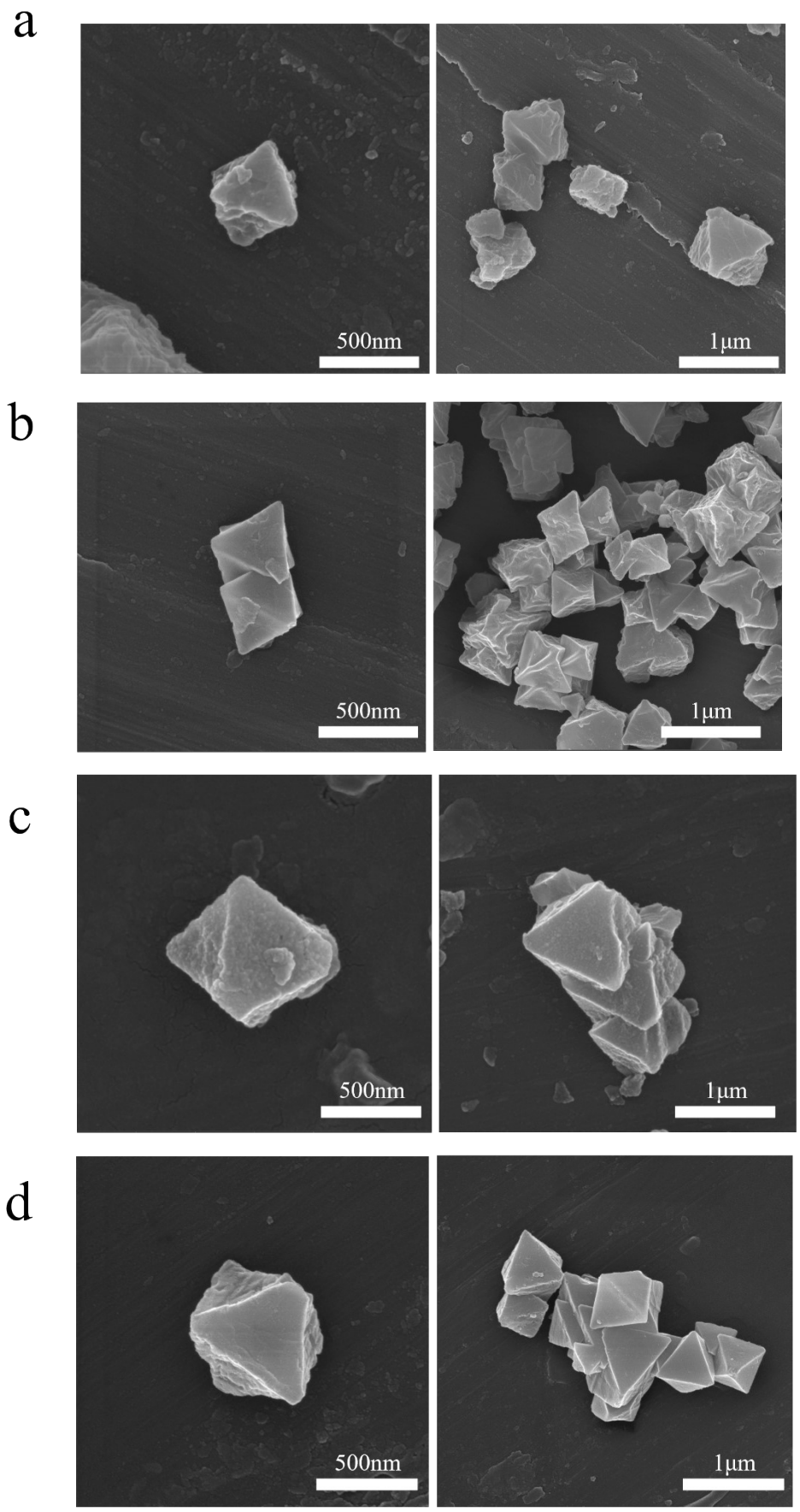

Figure S15. LC-MS/MS chromatogram showing the retention times of the five perfluorocarboxylic acids: PFOA (3.50 min), PFHpA (3.2 min), PFHxA (2.87 min), PFPeA (2.47 min), and PFBA (1.87 min).

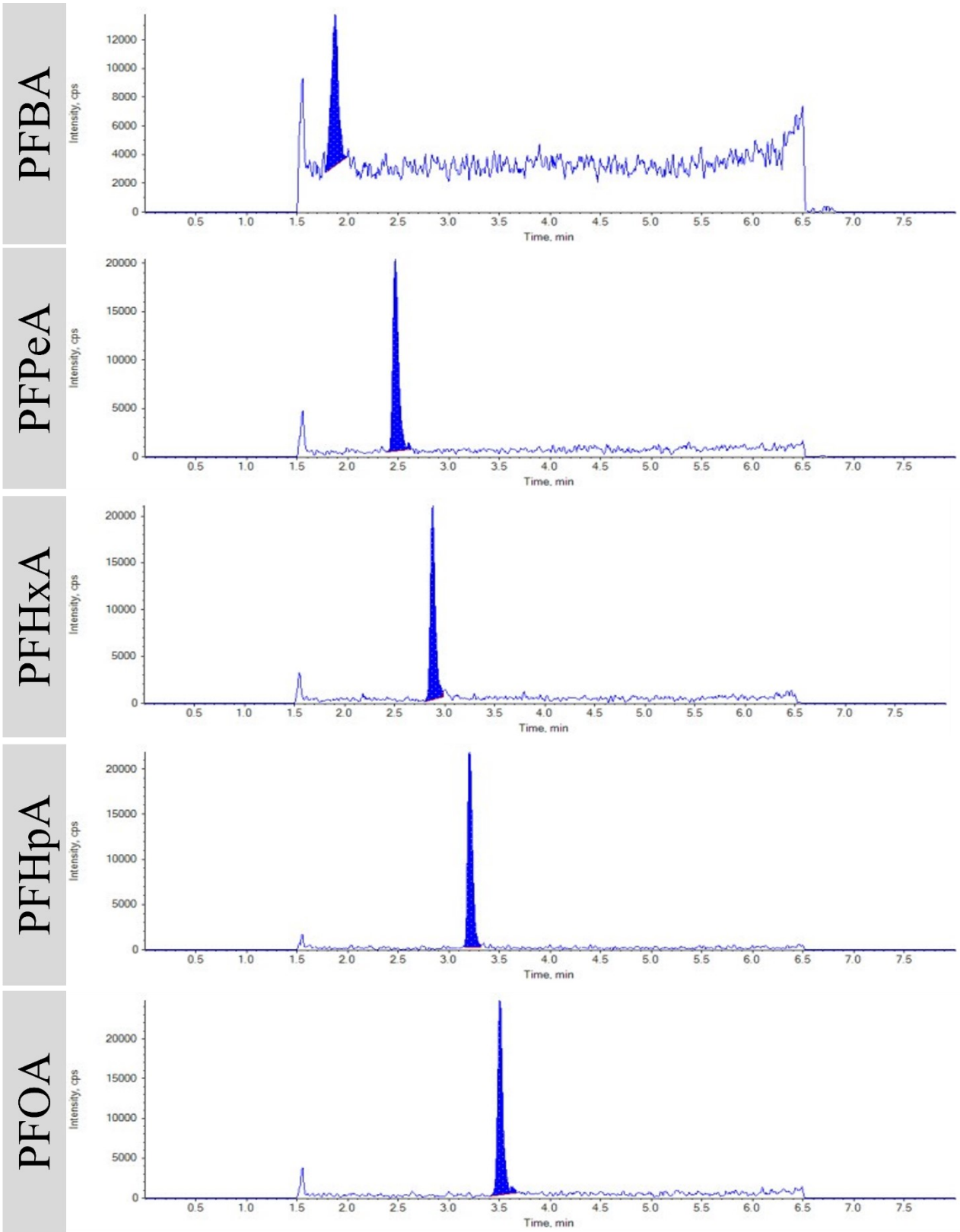

Figure S16 Kinetic fitting of (a) PFOA, (b) PFHxA, and (c) PFBA adsorption on MOF-808, MOF-808-Ala, MOF-808-PFPA, and MOF-808-TFMA.

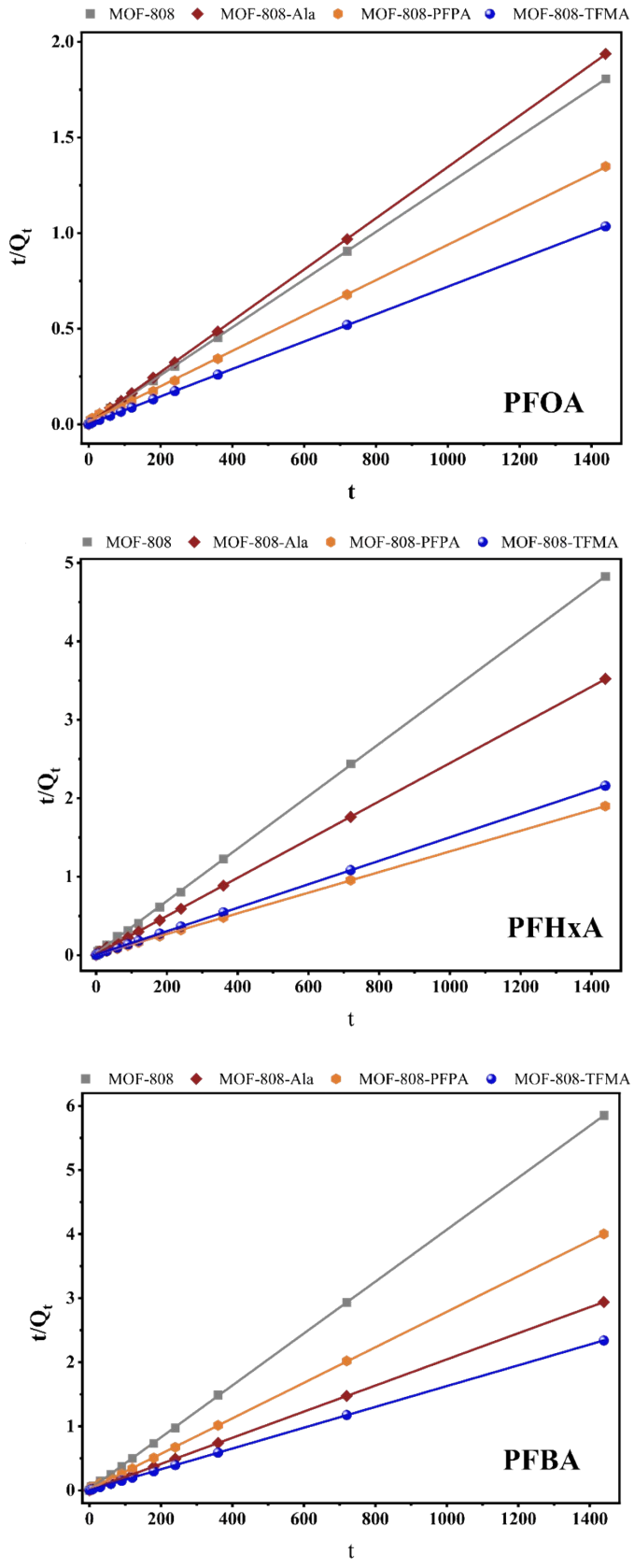

Figure S17. Adsorption isotherms of PFOA, PFHxA, and PFBA on MOF-808-TFMA at 288.15 K and 308.15 K, fitted with the Langmuir model.

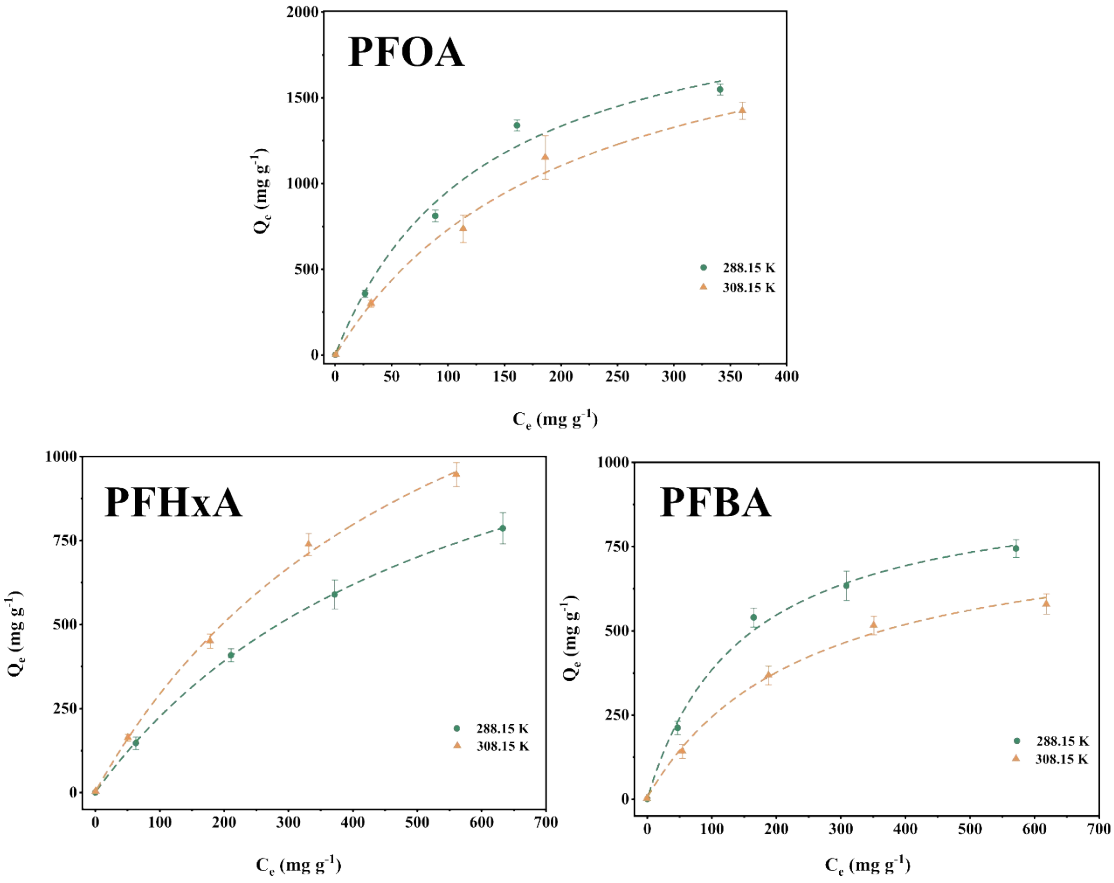

Figure S18. Relationship between ln K and 10^3/T for the adsorption of PFOA, PFHxA, and PFBA on MOF-808-TFMA.

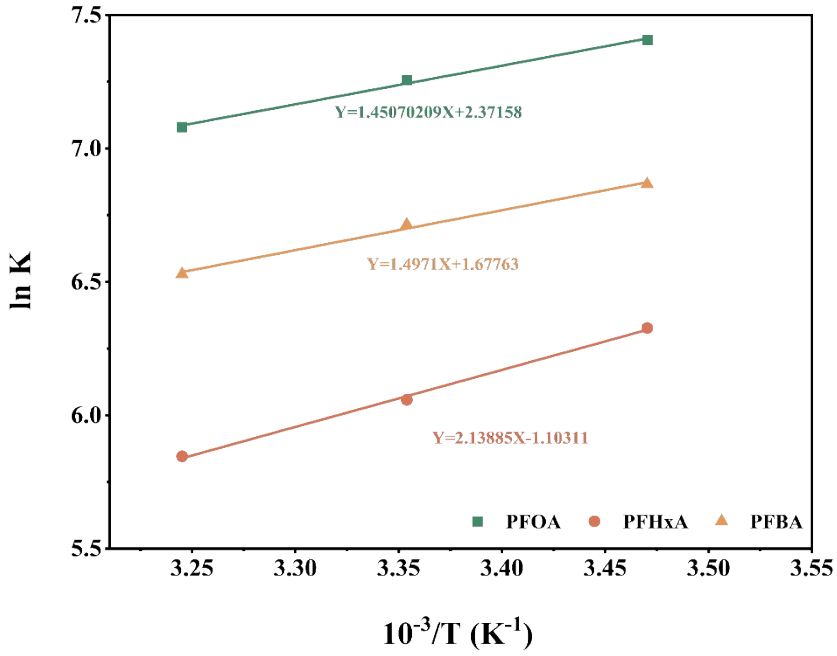

Figure S19. Effect of solution pH on the removal efficiency of PFHxA .

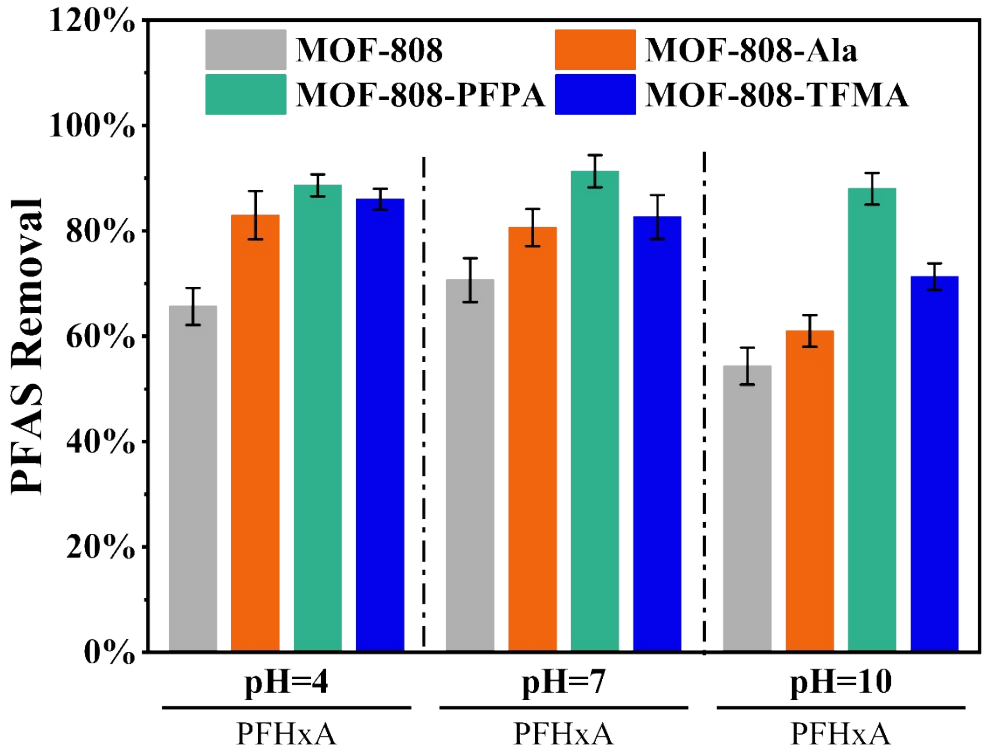

Figure S20. Removal efficiency of PFHxA by the adsorbent in pure water, and in the presence of inorganic anions and natural organic matter (NOM)

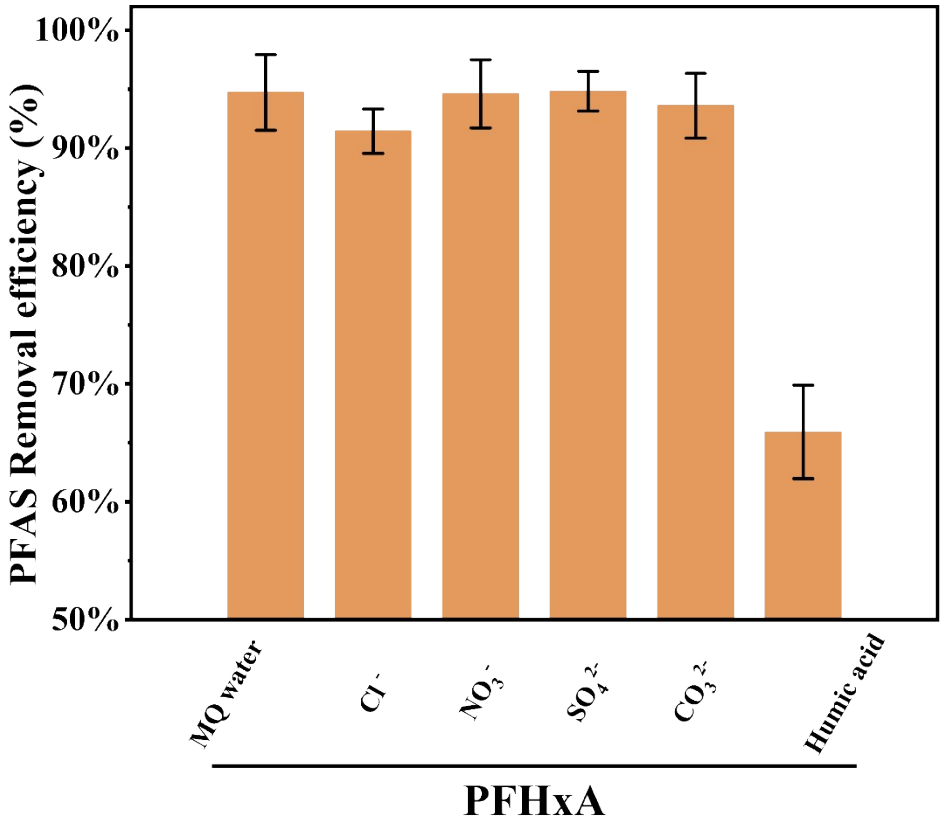

Figure S21. Removal performance of the adsorbent for trace-level PFAS in a tap water matrix

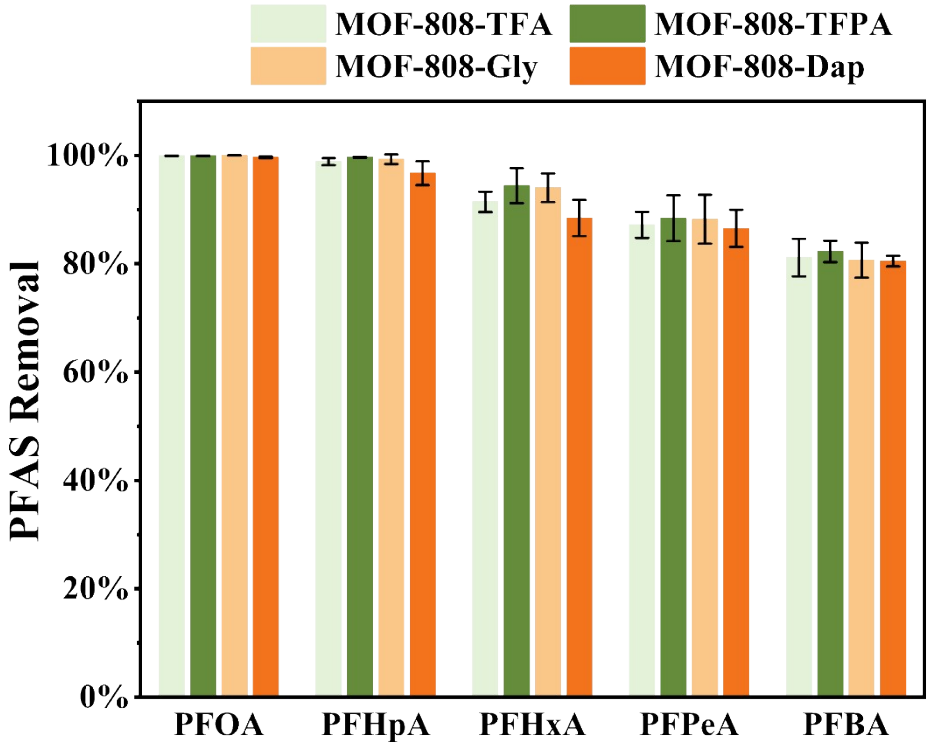

Figure S22 FT-IR spectra of MOF-808-Ala and MOF-808-PFPA before and after PFAS adsorption.

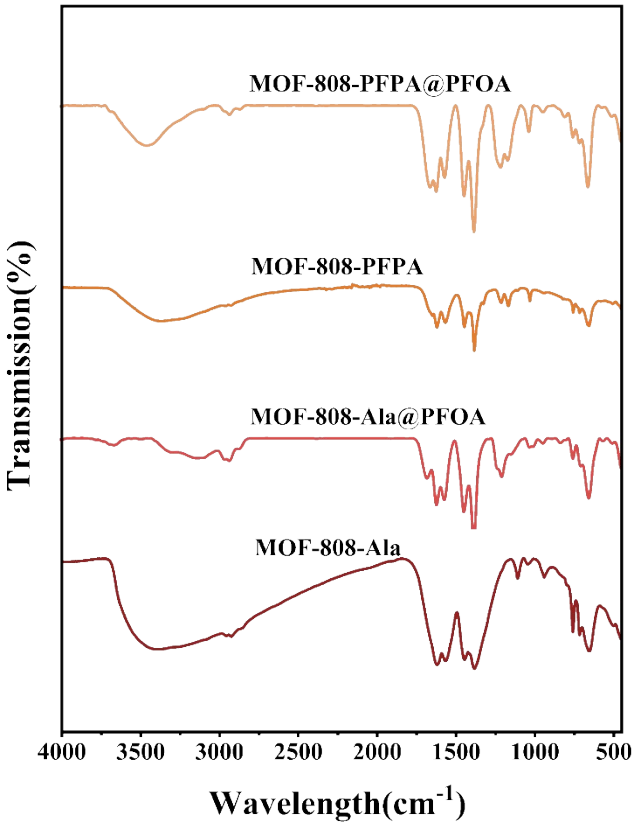

Figure S23. Pore size distributions of MOF-808 and MOF-808-TFMA after PFAS adsorption.

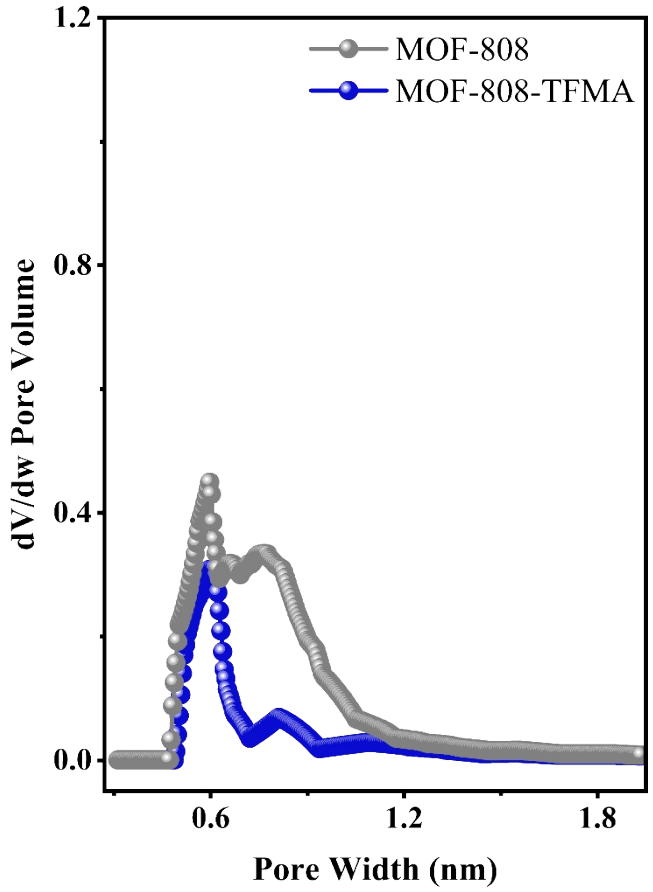

Figure S24. Electrostatic potential (ESP) distribution of MOF-808-Ala and MOF-808-PFPA.

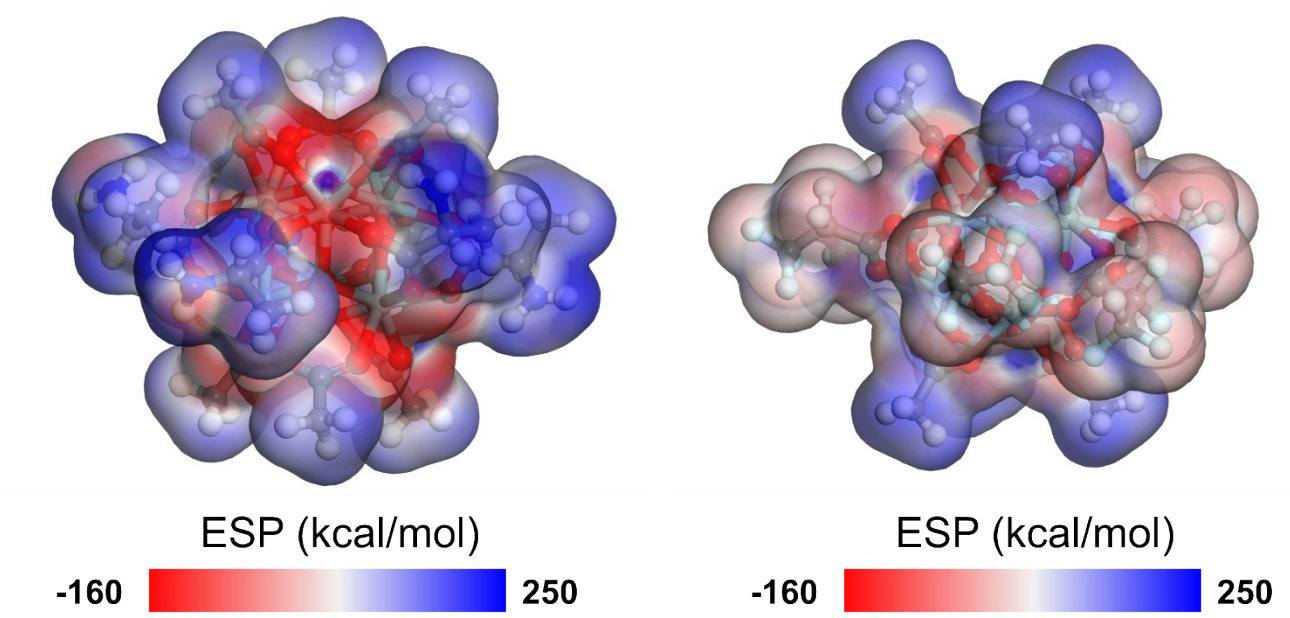

Figure S25. Adsorption energies of PFBA, PFHxA, and PFOA on MOF-808-Ala and MOF-808-PFPA.

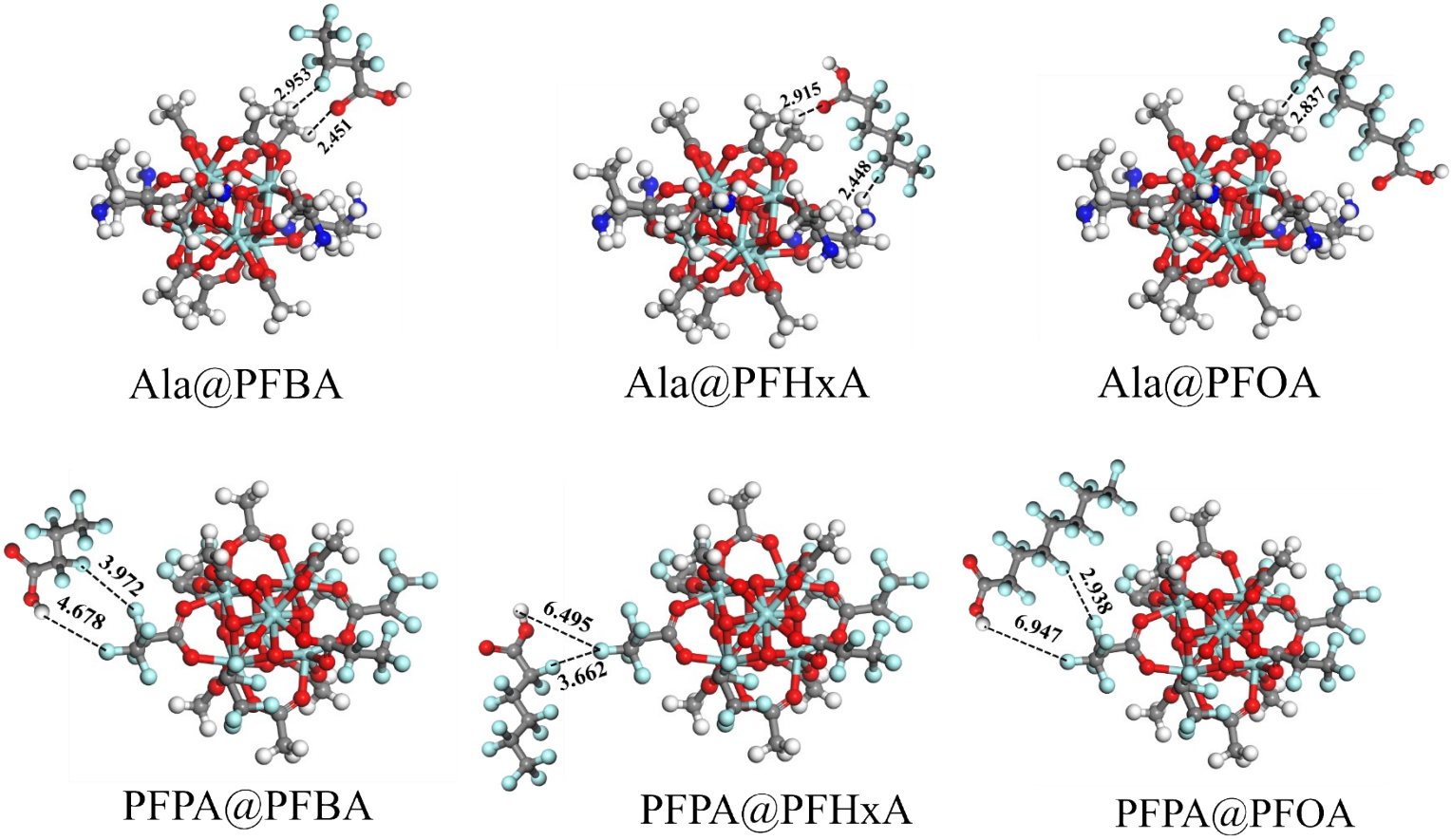

Figure S26. Adsorption energy of H^+ on MOF-808-TFMA.

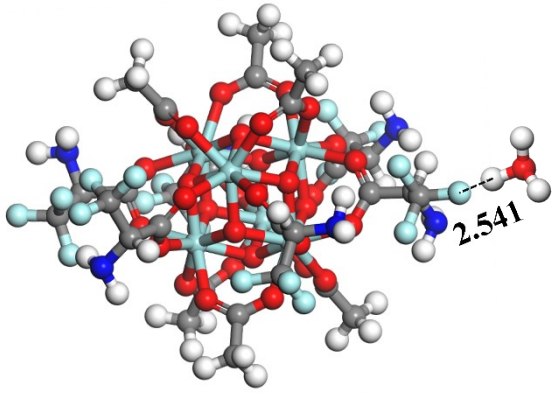

TFMA@H^+

E_{ads}= -94.52 KJ mol^{-1}

Table S1. Mass spectrometry parameters of five perfluorochemicals and their corresponding internal standards

Analytes	Precursor (m/z)	Production (m/z)	Declustering Potential(V)	Collision energy (V)
PFBA	213.0	168.9	-19	-13
PFPeA	263.0	218.9	-26	-11
PFHxA	312.9	268.9	-11	-11
PFHpA	362.9	318.9	-20	-14
PFOA	412.9	368.9	-30	-15
$^{13}C_4$-PFBA	217.0	172.9	-14	-24
$^{13}C_5$-PFPeA	268.0	223.9	-11	-20
$^{13}C_5$-PFHxA	318.9	274.9	-14	-21
$^{13}C_4$-PFHpA	368.9	321.9	-14	-21
$^{13}C_8$-PFOA	421.0	376.9	-13	-18

Table 2. Regression equations, correlation coefficients, detection limits, quantification limits and matrix effects evaluation of target perfluorochemicals

Analytes	Equation	R^2	LOD	LOQ	Reproducibility (RSD%, n=5)
PFBA	y=1010.694x-104.828	0.9976	0.10	0.30	9.1
PFPeA	y=1154.654x-55.838	0.9982	0.11	0.26	6.3
PFHxA	y=1077.480x-73.312	0.9979	0.18	0.54	6.9
PFHpA	y=1098.257x-63.872	0.9979	0.50	1.50	5.3
PFOA	y=1120.519x-193.022	0.9977	0.20	0.60	4.9

Table S3. Summary of experimental conditions for all conducted experiments and the PFAS species investigated in each experiment.

Experiment type	Initial concentration	PFAS species	Adsorbent quality/Volume	Adsorption time	PFAS mixed type
Batch removal	500 mg/L	PFOA ,PFHpA ,PFHxA , PFPeA , PFBA	5 mg/20 mL	12 h	Separate experiments
Adsorption kinetics	500 mg/L	PFOA , PFHxA ,PFBA	10 mg/40 mL	24 h	Separate experiments
Different pH values	5 μg/L	PFOA, PFHxA, PFBA	10 mg/40 mL	24 h	Separate experiments
Selective removal	10 μg/L	PFOA , PFHxA, PFBA	10 mg/40 mL	24 h	Separate experiments
Trace removal	5 μg/L	PFOA ,PFHpA ,PFHxA , PFPeA , PFBA	20 mg/40 mL	24 h	Mixture
Adsorption isotherm	100, 300, 500, 700 mg/L	PFOA , PFHxA ,PFBA	5 mg/20 mL	24 h	Separate experiments
Regeneration	10 μg/L	PFOA , PFBA	10 mg/25 mL	1 h	Mixture

Table S4. Pore volume, specific surface area, loading number per SBU, and gravimetric loading amount.

Types of MOF	Pore volume (cm^3 /g)	BET surface area (m^2/g)	The loading number of per SBU	Loaded capacity (mmol/L)
MOF-808	0.548	1650.76	NA	NA
MOF-808-FR	0.556	1708.483	NA	NA
MOF-808-Gly	0.338	900.968	4.17	2.83
MOF-808-Ala	0.150	420.179	2.24	1.57
MOF-808-Dap	0.138	377.152	3.39	2.20
MOF-808-TFA	0.406	1228.994	5.86	3.31
MOF-808-TFPA	0.372	1143.749	2.43	1.59
MOF-808-PFPA	0.314	910.734	1.87	1.20
MOF-808-TFMA	0.346	617.610	2.48	1.58

Table S5. Adsorption capacities of the MOF library for single-solute PFAS in deionized water.

Adsorbent	PFOA Capacity (mg/g)	PFHpA Capacity (mg/g)	PFHxA Capacity (mg/g)	PFPeA Capacity (mg/g)	PFBA Capacity (mg/g)
MOF-808	795.160	466.316	280.057	160.423	249.093
MOF-808-Gly	539.454	749.722	458.057	512.308	399.431
MOF-808-Ala	776.117	773.284	495.368	343.380	477.521
MOF-808-Dap	834.035	895.763	674.583	786.500	514.771
MOF-808-TFA	1557.785	768.098	574.471	493.424	372.662
MOF-808-TFPA	831.673	628.191	405.428	321.840	266.148
MOF-808-PFPA	1070.248	900.044	702.546	675.851	347.059
MOF-808-TFMA	1253.264	1025.334	652.691	769.764	684.562

Table S6. Data from the Langmuir and Freundlich adsorption isotherm models and the corresponding adsorption coefficients (K_d).

Sorbate	PFOA					PFHxA					PFBA				
	Langmuir	Freundlich				Langmuir	Freundlich				Langmuir	Freundlich			
Sorbent	R^2	R^2	N	K_F [$g^{n}\,L^{1-n}\,mg^{-1}$]	K_d [$L\,Kg^{-1}$]	R^2	R^2	N	K_F [$g^{n}\,L^{1-n}\,mg^{-1}$]	K_d [$L\,Kg^{-1}$]	R^2	R^2	N	K_F [$g^{n}\,L^{1-n}\,mg^{-1}$]	K_d [$L\,Kg^{-1}$]
MOF-808	0.986	0.961	1.288	8.548	3.171×10^{5}	0.999	0.998	1.482	5.67153	1.355×10^{5}	0.924	0.956	1.331	7.93908	1.165×10^{5}
MOF-808-Ala	0.967	0.987	1.537	15.928	4.111×10^{5}	0.958	0.971	1.529	7.36105	1.745×10^{5}	0.994	0.977	1.345	6.2441	2.016×10^{5}
MOF-808-PFPA	0.988	0.986	1.343	12.753	4.736×10^{5}	0.999	0.993	1.369	8.70442	2.808×10^{5}	0.953	0.973	1.368	8.70442	1.096×10^{5}
MOF-808-TFMA	0.993	0.953	1.548	39.572	1.124×10^{6}	0.997	0.999	1.373	7.97976	2.592×10^{5}	0.999	0.973	1.679	20.018	3.843×10^{5}

Table S7. Thermodynamic parameters for the adsorption of PFOA, PFHxA, and PFBA on MOF-808-TFMA at different temperatures.

PFOA			
T (K)	K_L (L/mg)	Ln(K)	ΔG° (KJ/mol)
288.15	0.00399	7.410	-17.752
298.15	0.00342	7.256	-17.986
308.15	0.00285	7.074	-18.122
ΔH° (KJ/mol)		-12.061	
ΔS° (J/mol K)		19.717	

PFHxA			
T (K)	K_L (L/mg)	Ln(K)	ΔG° (KJ/mol)
288.15	0.00178	6.328	-15.155
298.15	0.00136	6.057	-15.014
308.15	0.00110	5.845	-14.974
ΔH° (KJ/mol)		-17.782	
ΔS° (J/mol K)		-10.540	

PFBA			
T (K)	K_L (L/mg)	Ln(K)	ΔG° (KJ/mol)
288.15	0.00448	6.886	-16.448
298.15	0.00385	6.714	-16.643
308.15	0.00320	6.528	-16.724
ΔH° (KJ/mol)		-12.447	
ΔS° (J/mol K)		13.948	

Table S8. Specified recovery results of blank experiments: The recovery rate of the target PFAS on the polypropylene bottle and the nylon filter.

Target PFAS	**Spiked Concentration (µg/L)**	**Average Recovery Rate (%)**	**Relative Standard Deviation (RSD, %, n=3)**
PFBA	5	97.4%	1.45
	10	99.3%	0.43
PFPeA	5	98.9%	0.33
	10	99.8%	0.10
PFHxA	5	99.1%	0.19
	10	99.2%	0.03
PFHpA	5	98.9%	0.65
	10	99.6%	0.02
PFOA	5	97.4%	1.02
	10	99.1%	0.52

Table S9. Comparison of PFAS adsorption capacities between MOF-808-TFMA and conventional adsorbents and other MOFs.

adsorbing materials	PFAS tested	PFAS concentration (mg/L)	PFAS adsorption Capacity (mg/g)	Reference
GAC(F400)	PFOA, PFPeA	415,265	161,34	[3]
SMC(FS200)	PFOA, PFPeA	415,265	108,42	[3]
AER(CalRes2301)	PFOA, PFPeA	415,265	559,214	[3]
MIL-101-Cr	PFOA	1000	460	[4]
MIL-101-Cr-NH_2	PFOA	1000	290	[4]
MIL-101-Cr-NMe_3	PFOA	1000	493	[4]
MIL-101-Cr-DMEN	PFOA	1000	534	[4]
MIL-808-Cr-QDMEN	PFOA	1000	754	[4]
UIO-66	PFOA	500	388	[5]
UIO-67	PFOA	500	743	[5]
UIO-66-F4	PFOA	500	467	[6]
Fe-BTC	PFOA	1000	548	[7]
Mn-BTC	PFOA	1000	130	[7]
Cu-BTC	PFOA	1000	95	[7]
Ce-BTC	PFOA	1000	210	[7]
NU-1000	PFOA,PFHpA, PFPeA,PFBA	0.1-1000	507,421,344,274	[8]
MOF-808-TFA	PFOA,PFHxA, PFBA	100-800	1341,436,311	[9]
PCN-999	PFOA,PFBA	100-5000	1089,247	[10]
MOF-808-TFMA	PFOA,PFHxA, PFBA	100-700	1558,826, 606	This work
PCN-1002	PFOA	1000	632	[11]
PCN-1003	PFOA,PFBA	1000	836,642	[12]
Zn (aIM + bIM)	PFBA	100	439	[13]

Reference

1. H. Furukawa, F. Gándara, Y.-B. Zhang, J. Jiang, W. L. Queen, M. R. Hudson and O. M. Yaghi, *J. Am. Chem. Soc.*, 2014, **136**, 4369–4381.
2. H. Lyu, O. I.-F. Chen, N. Hanikel, M. I. Hossain, R. W. Flaig, X. Pei, A. Amin, M. D. Doherty, R. K. Impastato, T. G. Glover, D. R. Moore and O. M. Yaghi, *J. Am. Chem. Soc.*, 2022, **144**, 2387–2396.
3. E. R. Pezoulas, B. Tajdini, Y. Ko, A. A. Uliana, R. Giovine, H. Furukawa, H. Vatankhah, J. Börgel, K. C. Kim, C. Bellona and J. R. Long, *J. Am. Chem. Soc.*, 2025, **147**, 21832–21843.
4. K. Liu, S. Zhang, X. Hu, K. Zhang, A. Roy and G. Yu, *Environ. Sci. Technol.*, 2015, **49**, 8657–8665.
5. K. Sini, D. Bourgeois, M. Idouhar, M. Carboni and D. Meyer, *Mater. Lett.*, 2019, **250**, 92-95.
6. K. Sini, D. Bourgeois, M. Idouhar, M. Carboni and D. Meyer, *New J. Chem.*, 2018, **42**, 17889-17894.
7. Y. Yang, Z. Zheng, W. Ji, J. Xu and X. Zhang, *J. Hazard. Mater.*, 2020, **395**.
8. R. Li, S. Alomari, R. Stanton, M. C. Wasson, T. Islamoglu, O. K. Farha, T. M. Holsen, S. M. Thagard, D. J. Trivedi and M. Wriedt, *Chem. Mater.*, 2021, **33**, 3276–3285.
9. E. Loukopoulos, S. Marugán-Benito, D. Raptis, E. Tylianakis, G. E. Froudakis, A. Mavrandonakis and A. E. Platero-Prats, *Adv. Funct. Mater.*, 2024, **34**.
10. R.-R. Liang, S. Xu, Z. Han, Y. Yang, K.-Y. Wang, Z. Huang, J. Rushlow, P. Cai, P. Samorì and H.-C. Zhou, *J. Am. Chem. Soc.*, 2024, **146**, 9811–9818.
11. R. R. Liang, Y. Yang, Z. Han, V. I. Bakhmutov, J. Rushlow, Y. Fu, K. Y. Wang and H. C. Zhou, *Adv. Mater.*, 2024, **36**.
12. R.-R. Liang, Y. Fu, Z. Han, Y. Yang, V. I. Bakhmutov, Z. Liu, J. Rushlow and H.-C. Zhou, *Nature Water*, 2024, **2**, 1218–1225.
13. Y. Sun, K. Quan, J. He, J. Chen, Z. Li and H. Qiu, *Chem. Eng. J.*, 2024, **495**.